Long-lasting blood-brain barrier dysfunction and neuroinflammation after traumatic brain injury

van Vliet, E.A.; Ndode-Ekane, X.E.; Lehto, L.J.; Gorter, J.A.; Andrade, P.; Aronica, E.; Gröhn, O.; Pitkänen, A.

DOI
10.1016/j.nbd.2020.105080

Publication date
2020

Document Version
Final published version

Published in
Neurobiology of Disease

Neurobiology of Disease 145 (2020) 105080

Contents lists available at ScienceDirect

Neurobiology of Disease

journal homepage: www.elsevier.com/locate/ynbdi

Long-lasting blood-brain barrier dysfunction and neuroinflammation after traumatic brain injury

Erwin A. van Vliet[a,b,*], Xavier Ekolle Ndode-Ekane[c], Lauri J. Lehto[c], Jan A. Gorter[a], Pedro Andrade[c], Eleonora Aronica[b,d], Olli Gröhn[c], Asla Pitkänen[c]

[a] Center for Neuroscience, Swammerdam Institute for Life Sciences, University of Amsterdam, Amsterdam, the Netherlands
[b] Department of (Neuro)Pathology, Amsterdam UMC, University of Amsterdam, Amsterdam, Amsterdam Neuroscience, the Netherlands
[c] A. I. Virtanen Institute for Molecular Sciences, University of Eastern Finland, Kuopio, Finland
[d] Stichting Epilepsie Instellingen Nederland (SEIN), Heemstede, the Netherlands

ARTICLE INFO

Keywords:
Epilepsy
Epileptogenesis
Gadolinium
Contrast-enhance magnetic resonance imaging
Perilesional cortex
Thalamus

ABSTRACT

Background: Traumatic brain injury (TBI) causes 10–20% of acquired epilepsy, which typically develops within 2 years post-injury with poorly understood mechanisms. We investigated the location, severity, evolution and persistence of blood-brain barrier (BBB) dysfunction and associated neuroinflammation after TBI, and their contribution to post-traumatic seizure susceptibility.

Methods: TBI was induced with lateral fluid-percussion in adult male Sprague-Dawley rats (6 sham, 12 TBI). Permeability of the BBB was assessed using T1-weighted magnetic resonance imaging (MRI) with gadobutrol (Gd) contrast enhancement at 4 days, 2 weeks, 2 months, and 10 months post-injury and with intravenously administered fluorescein at 11 months post-TBI. Continuous (24/7) video-EEG monitoring was performed for 3 weeks at 11 months post-injury followed by the pentylenetetrazol (PTZ) seizure-susceptibility test. In the end, rats were perfused for histology to assess albumin extravasation, iron deposits, calcifications, reactive astrocytes, microglia and monocytes. To investigate the translational value of the data obtained, BBB dysfunction and neuroinflammation were investigated immunohistochemically in autopsy brain tissue from patients with TBI and PTE.

Results: MRI indicated persistent Gd leakage in the impacted cortex and thalamus of variable severity in all rats with TBI which correlated with fluorescein extravasation. In the impacted cortex BBB dysfunction was evident from 4 days post-injury onwards to the end of the 10-months follow-up. In the ipsilateral thalamus, leakage was evident at 2 and 10 months post-injury. The greater the BBB leakage in the perilesional cortex at 10 months after the injury, the greater the expression of the endothelial cell antigen RECA-1 ($r = 0.734$, $p < 0.01$) and the activated macrophages/monocytes/microglia marker CD68 ($r = 0.699$, $p < 0.05$) at 11 months post-injury. Seven of the 12 rats with TBI showed increased seizure susceptibility in the PTZ-test. Unlike expected, we did not find any association between increased Gd-leakage or neuroinflammation with seizure susceptibility at 11 months post-TBI. Analysis of human autopsy tissue indicated that similar to the animal model, chronic BBB dysfunction was also evident in the perilesional cortex and thalamus of patients with PTE, characterized by presence of albumin, iron deposits and calcifications as well as markers of neuroinflammation, including reactive astrocytes, microglia and monocytes.

Conclusions: Rats and humans with TBI have long-lasting cortical BBB dysfunction and neuroinflammation. Focal Gd-enhancement matched with loci of neuroinflammation, particularly in the thalamus. Although BBB leakage did not associate with increased seizure susceptibility after TBI, our data suggest that for treatments aimed to mitigate BBB damage and its secondary pathologies like chronic neuroinflammation, there is a region-specific, long-lasting therapeutic time window.

Abbreviations: BBB, blood-brain barrier; CE-MRI, contrast-enhanced magnetic resonance imaging; DAPI, 4′,6-diamidino-2-phenylindole; Gd, gadobutrol; FSC, fluorescein; KPBS, potassium phosphate-buffered saline; LFP, lateral fluid percussion; NHS, normal horse serum; PTZ, pentylenetetrazole; PTE, post-traumatic epilepsy; RECA, rat endothelial cell antigen; ROC, receiver operating characteristic; ROI, region of interest; RT, room temperature; SWD, spike-wave discharge; TBI, traumatic brain injury; VPM, ventral posteromedial; VPL, ventral posterolateral

* Corresponding author at: Center for Neuroscience, Swammerdam Institute for Life Sciences, University of Amsterdam, P.O. box 94246, 1090 GE, Amsterdam, the Netherlands.
E-mail address: e.a.vanvliet@uva.nl (E.A. van Vliet).

https://doi.org/10.1016/j.nbd.2020.105080
Received 24 May 2020; Received in revised form 16 August 2020; Accepted 5 September 2020
Available online 09 September 2020

1. Introduction

Traumatic brain injury (TBI) refers to an alteration in brain function, or other evidence of brain pathology, caused by an external force (Menon et al., 2010). It is a major cause of long-lasting quality-of-life compromising psychiatric and neurological morbidities, including post-traumatic epilepsy (PTE) (Annegers et al., 1998; Perry et al., 2017). Major preclinical attempts have been made to improve the post-TBI outcome by targeting various cellular components of the secondary damage, including neurodegeneration, axonal injury, oxidative stress and neuroinflammation (Marklund and Hillered, 2011; Xiong et al., 2013). Yet, treatments to improve post-TBI functional outcome are not available (Kim et al., 2019).

More recently, damage to the blood-brain-barrier (BBB), composed of endothelial cells, pericytes, astrocytes, and basal lamina, has been indicated as a major contributor to maintenance of chronic inflammation after brain injury (Bar-Klein et al., 2017; Obermeier et al., 2016). Accordingly, acute treatments restoring the function of the BBB have shown promise in improving short-term post-TBI outcome in animal models (Thal and Neuhaus, 2014). However, the time window of post-TBI BBB impairment and its location(s) are still poorly understood, even though such information would be critical for tailoring the duration of treatment in affected brain areas. Moreover, the temporo-spatial co-occurrence of BBB dysfunction with the inflammatory tissue response has been little studied, even though co-targeting of both pathologies within an optimal time window would present an appealing strategy to improve post-TBI outcome.

We have recently developed a sensitive contrast-enhancement magnetic resonance imaging (MRI) based method that non-invasively detects BBB dysfunction in vivo (van Vliet et al., 2014b). The protocol includes a step-down infusion, which can detect subtle BBB leakage in rodents after brain insults. This and other studies have shown that BBB dysfunction and consequent brain inflammation can enhance seizure susceptibility in animal models of epileptogenesis induced by status epilepticus (SE), focal cortical injury or lateral fluid-percussion -induced TBI and also in human temporal lobe epilepsy and PTE (Frey et al., 2014; Ivens et al., 2007; Michalak et al., 2012; Tomkins et al., 2008; Van Vliet et al., 2007).

Here, our objective was to assess the temporo-spatial evolution of BBB dysfunction and its persistence over a 1-year follow-up after lateral fluid-percussion -induced TBI. Moreover, we investigated the association of BBB dysfunction with chronic neuroinflammation and increased seizure-susceptibility at 11 months post-TBI.

An important issue to consider when studying pathophysiological mechanisms in animal models, is the translation from the animal model to the human condition. Although many medical therapies that are used in the clinic today have been initially tested in animals, animal studies often fail to replicate in clinical trials. This can be due to species differences or differences in pathophysiology, disease etiology, onset or progression. Therefore, it is of crucial importance to compare findings in the animal model to the human situation. The lateral fluid-percussion injury model is the most widely used and investigated model for human closed head injury and mimics many of the neuropathological alterations that are found in the epileptogenic human brain (Pitkänen and McIntosh, 2006). To investigate the translational value of the data obtained in this model, BBB dysfunction and neuroinflammation were investigated immunohistochemically in autopsy brain tissue from patients with TBI and PTE. We hypothesized that the progression of BBB dysfunction will be brain area-dependent. Further, chronic BBB dysfunction will associate with chronic neuroinflammation and increased seizure susceptibility.

2. Materials and methods

The study design is summarized in Fig. 1A.

2.1. Animals

A total of 22 adult male Sprague-Dawley rats [average body weight at the time of injury 465 g (range 388-537 g); Charles River, Sulzfeld, Germany)] were used. All rats were individually housed in a controlled environment (temperature 22 ± 1 °C; humidity 50–60%; lights on from 07:00 to 19:00 h). Pellet food and water were provided ad libitum. All animal procedures were approved by the Animal Ethics Committee of the Provincial Government of The Southern Finland and carried out in accordance with the guidelines of the European Community Council Directives 2010/63/EU.

2.2. Induction of traumatic brain injury with lateral fluid-percussion

The procedure for induction of lateral fluid-percussion injury (FPI) has been described previously (Kharatishvili et al., 2006; McIntosh et al., 1989). In brief, animals (n = 22) were anesthetized with an intraperitoneal (i.p.) injection of a solution (6 ml/kg) containing sodium pentobarbital (58 mg/kg), chloral hydrate (60 mg/kg), magnesium sulphate (127.2 mg/kg), propylene glycol (42.8%) and absolute ethanol (11.6%), and placed in a Kopf stereotactic frame (David Kopf Instruments, Tujunga, CA, USA). The skull was exposed with a midline skin incision and the periosteum was extracted. The left temporal muscle was gently detached from the lateral ridge. A circular craniectomy (Ø 5 mm) was performed using a hand-held trephine over the left parietal lobe midway between lambda and bregma (Fig. 2A). Care was taken to leave the dura intact. A saline filled female Luer-Lock fitting was sealed into the craniectomy with a glue (3 M Vetbond, 3 M Deutschland GmbH, Germany) and fixed to the skull with a supporting screw using dental acrylate (Selectaplus CN, Dentsply DeTrey GmbH, Dreieich, Germany). Severe TBI was induced 90 min after the induction of anesthesia by connecting the rat to a fluid-percussion device (AmScien Instruments, Richmond, VA, USA) via a Luer-Lock fitting. The mean severity of the impact was 3.00 ± 0.02 atm (min 2.92 - max 3.09 atm). Time in apnea and occurrence of acute post-impact seizure-like behavior were monitored. Sham-operated controls (n = 6) underwent anesthesia and all surgical procedures, except lateral FPI.

2.3. Magnetic resonance imaging

Each surviving rat (6 sham-operated, 12 TBI) was scanned under 1.0–1.5% isoflurane anesthesia in 30%/70% oxygen/nitrogen gas mixture at four time points after TBI (4 days, 2 weeks, 2 months, 10 months). Magnetic resonance imaging (MRI) was conducted using a 7 T horizontal scanner (Bruker PharmaScan) at 4 days, 2 weeks, and 2 months and using a 9.4 T horizontal scanner (Varian Inc., Palo Alto, CA) at 10 months post-TBI (since animals did not fit into the 7 T scanner anymore) interfaced to a Varian DirectDrive console (Varian Inc., Palo Alto, CA, USA). Radiofrequency transmission and signal reception were performed with a volume transmit/receive coil (Bruker). Our previous study in a status epilepticus rat model showed that a step-down infusion protocol with a T1-shortening contrast agent (gadobutrol, Gd) can be used to quantify BBB permeability after brain injury (van Vliet et al., 2014b). Briefly, T1-weighted MR images (gradient echo; repetition/echo time, 367/3 ms; flip angle, 70°; field of view, 3.2 × 1.6 cm^2; acquisition matrix, 256 × 128; slice thickness 1.0 mm, 19 consecutive slices covering the cerebrum; voxel resolution, 0.125 × 0.125 × 1 mm^3) were acquired before and 45 min after the beginning of a 20 min step-down infusion with 0.2 M Gd (diluted in 0.9% NaCl; Gadovist®, Schering, Kenilworth, NJ, USA). Gd-injection was done via the tail vein, using a syringe pump (Model PhD2000, Harvard Apparatus, South Natick, MA, USA) programmed to reach the highest possible stable Gd blood concentration during 20 min (van Vliet et al., 2014b). Contrast-induced signal changes were calculated from the scans taken before and after tracer infusion (van Vliet et al., 2014b). T2-weighted MR images (fast spin echo; repetition/effective echo time, 4000/50 ms; echo

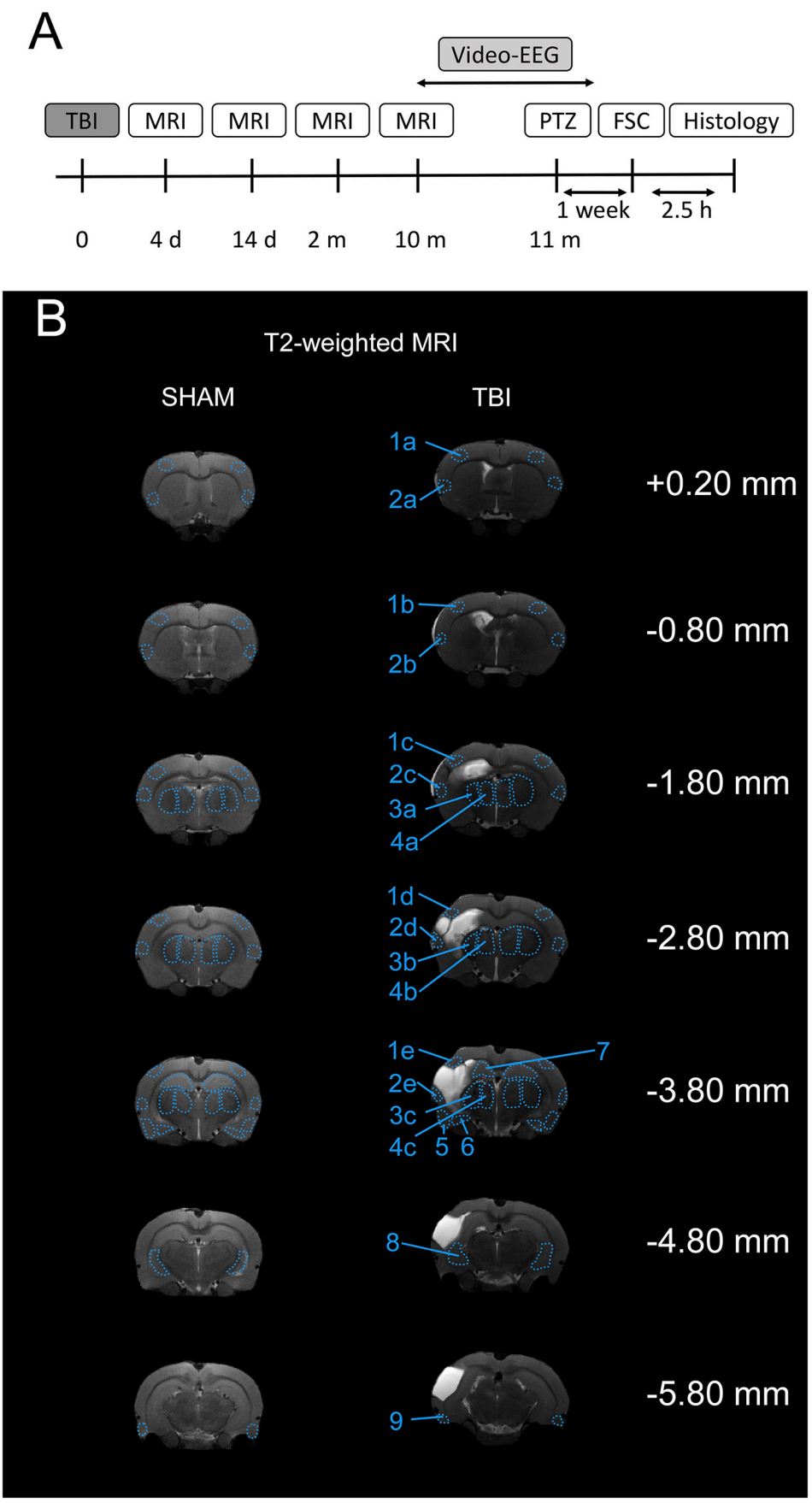

Fig. 1. Study design and selection of regions of interest using T2-weighted images. (A) In order to assess blood-brain-barrier (BBB) permeability, magnetic resonance imaging with gadobutrol (Gd) contrast enhancement was performed at 4 days, 2 weeks, 2 months, and 10 months after traumatic brain injury (TBI). After the last imaging session, rats were implanted with epidural skull electrodes, and continuous video-electroencephalogram (vEEG) recordings were performed for 3 weeks to observe the occurrence of spontaneous seizures. In the end, (i.e., 11 months after TBI), the pentyleneterazole (PTZ) test was performed to determine whether seizure susceptibility was increased after TBI. To validate the MRI data, a BBB tracer, fluorescein (FSC), was injected intravenously at 1 week after the PTZ test under vEEG, and animals were perfused for histological analysis 2.5 h later. (B) To assess the evolution and extent of BBB leakage, regions of interest (ROIs, blue dashed lines) were manually outlined at each time point on T2-weighted coronal images at different rostrocaudal levels [i.e., +0.20, −0.80, 1.80, 2.80, 3.80, 4.80, and 5.80 mm from the bregma, according to the rat brain atlas of Paxinos and Watson (2007), and transferred to the corresponding Gd-leakage maps. The following areas were analyzed both ipsilaterally and contralaterally: (1a-e) dorsal perilesional cortex; (2a-e) ventral perilesional cortex; (3a-c) lateral thalamus; (4a-c) medial thalamus; (5) amygdala; (6) piriform cortex; (7) septal hippocampus; (8) temporal hippocampus; (9) entorhinal cortex. T2 enhancement (with exclusion of ventricles) in the ipsilateral cortex was used to indicate the lesion area at each time point. T2-weighted images from a representative sham-operated animal (#e28) are shown on the left and from a rat with TBI (#e25, MRI at 10 months post-TBI) on the right. (For interpretation of the references to colour in this figure legend, the reader is referred to the web version of this article.)

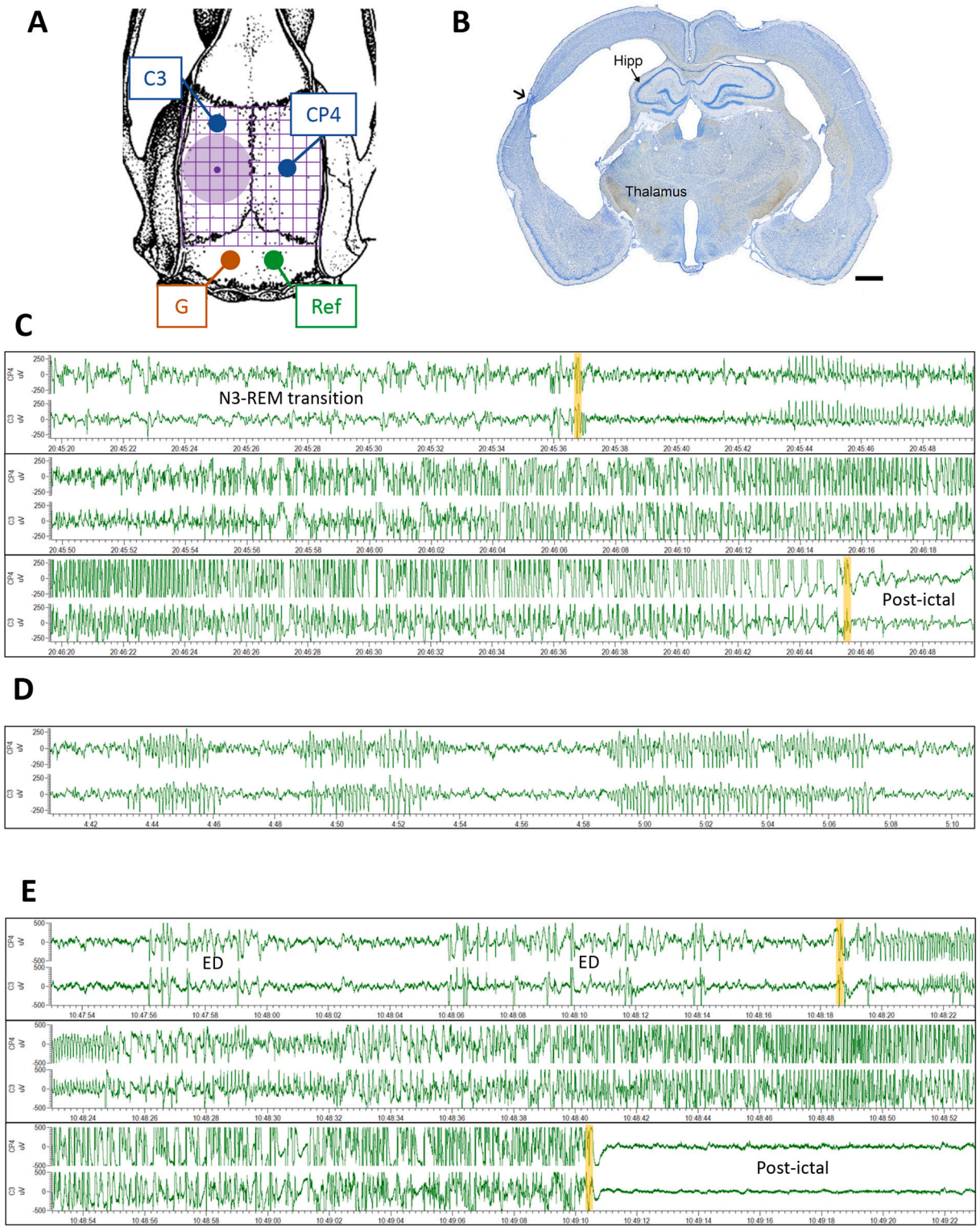

Fig. 2. Phenotyping of epilepsy and seizure-susceptibility at 10 months after traumatic brain injury (TBI). (A) Location of the craniotomy (purple circle) and two epidural recording (blue; C3, CP4), a reference (green; Ref), and a ground (brown; G) screw electrodes in the skull. Grid dimensions are 1 mm × 1 mm. (B) A representative thionin-stained coronal section from the level of the TBI lesion core in a rat with epilepsy (#e16). Arrow points to lesion core. Scalebar = 1 mm. (C) An unprovoked late secondarily generalized seizure in rat #e16 at 10 months post-TBI. Letters on the left refer to the electrode placements shown in panel A. Yellow bars indicate the beginning and the end of the seizure. Note that the seizure started at the N3-REM (rapid-eye-movement) transition. (D) A spike-wave discharge (SWD) in rat #e16. In line with previous studies (Kadam et al., 2017; Rodgers et al., 2015; Taylor et al., 2019, 2017), SWDs were not counted as TBI-related seizures. (E) A pentylenetetrazol (PTZ)-induced seizure preceded by PTZ-induced epileptiform discharges (ED) in rat #e16. (For interpretation of the references to colour in this figure legend, the reader is referred to the web version of this article.)

spacing, 25 ms; field of view, 3.2 × 1.6 cm^2; acquisition matrix, 256 × 128; slice thickness 1.0 mm, 19 consecutive slices covering the cerebrum; voxel resolution, 0.125 × 0.125 × 1 mm^3) were acquired. Regions of interest (ROIs) were outlined manually (Fig. 1B) at different coronal levels [i.e., +0.20, −0.80, 1.80, 2.80, 3.80, 4.80 and 5.80 mm from the bregma; (Paxinos and Watson, 2007)], and transferred to Gd-leakage maps (Fig. 4).

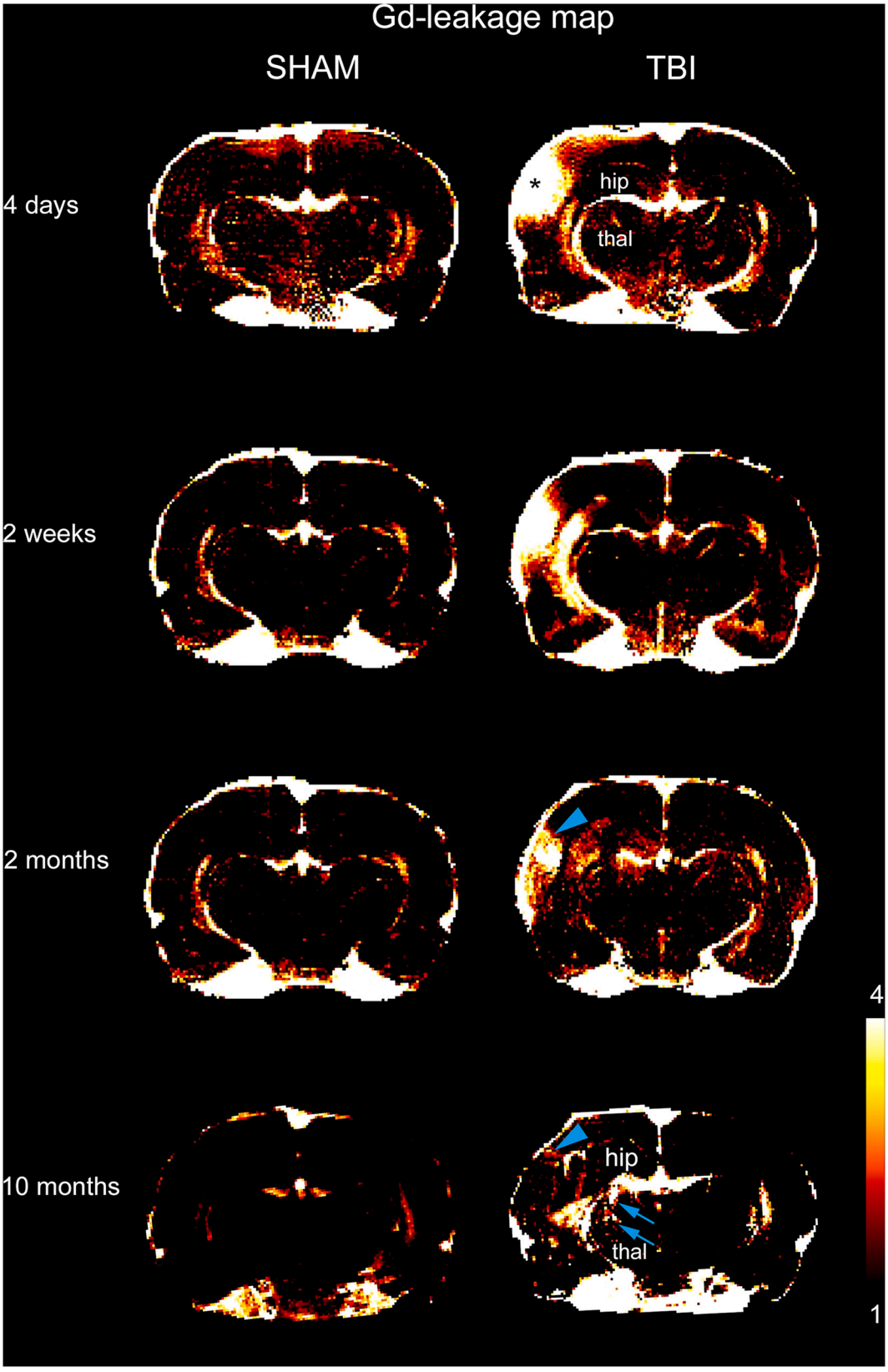

(caption on next page)

Fig. 3. Gadobutrol (Gd) leakage maps. Coronal images from representative cases show Gd-leakage in the brain at 4 days, 2 weeks, 2 months, and 10 months post-TBI. Gd-leakage was calculated as the relative signal enhancement induced by Gd accumulation: the pre-contrast T1-weighted signal intensity was subtracted from the post-contrast signal intensity and divided by the pre-contrast signal intensity, as previously described (van Vliet et al., 2014b). The closer the colour to white (i.e., the greater the number in the colour bar on the right lower corner), the greater the leakage. Gd-leakage was most robust in the lesioned ipsilateral cortex at 4 days post-TBI (asterisk). At 2 weeks post-TBI, Gd-leakage was still detectable in the lesion core and perilesional cortex, even though to a lesser extent as compared to that at 4 days post-TBI. Even at 2 months and 10 months post-TBI, Gd-leakage was still evident in the dorsal perilesional cortex (blue arrowheads). Interestingly, Gd-leakage was also evident in the lateral aspects of the ipsilateral thalamus, but not before 2 months post-TBI, becoming most evident at 10 months post-TBI (blue arrows). Gd-leakage was not detected in the ventral perilesional cortex, medial thalamus, amygdala, piriform cortex, hippocampus or entorhinal cortex of injured rats at any of the time points. Abbreviations: hip, hippocampus; TBI, traumatic brain injury; thal, thalamus. (For interpretation of the references to colour in this figure legend, the reader is referred to the web version of this article.)

2.4. MRI analysis

The following brain areas were analyzed ipsilateral to lesion and in the corresponding contralateral area (see Fig. 1B): (**1a–e**) cortex dorsal to the lesion core (dorsal perilesional cortex); (**2a–e**) cortex ventral to the lesion core (ventral perilesional cortex); (**3a–c**) lateral thalamus; (**4a–c**) medial thalamus; (**5**) amygdala; (**6**) piriform cortex; (**7**) septal hippocampus; (**8**) temporal hippocampus; (**9**) entorhinal cortex. Gd-leakage was calculated as the relative signal enhancement induced by Gd accumulation. For each animal a Gd leakage map was created (Fig. 3) by digital subtraction of the pre-contrast T1-weighted signal intensity from the post-contrast signal intensity and divided by the pre-contrast signal intensity as previously described (van Vliet et al., 2014b). Voxels above a threshold of 0.2 were manually delineated by a researcher blinded to the group assignments and projected onto the Gd-leakage map as previously described (van Vliet et al., 2014b). For each ROI, the mean signal enhancement was calculated from the Gd-leakage map.

2.5. Video-EEG recordings

2.5.1. Electrode implantation

After the last imaging session at 10 months post-TBI, rats (6 sham-operated, 12 TBI) were anesthetized for electrode implantation with a single injection (6 ml/kg, i.p.) of a mixture containing sodium pentobarbital (58 mg/kg), chloral hydrate (60 mg/kg), magnesium sulphate (127.2 mg/kg), propylene glycol (42.8%), and absolute ethanol (11.6%). Animals were then mounted in a stereotactic frame with the lambda and bregma on the same horizontal level. Two screw electrodes (E363/20 Plastics One Inc., Roanoke, VA, USA) were inserted epidurally into the skull over the parietal cortex, one rostral to the craniectomy, and the other contralateral to the centre of the craniectomy (Fig. 2A). Two stainless steel cortical electrodes implanted into the skull bilaterally over the cerebellum served as reference and ground electrodes. Electrodes were fixed to the skull using dental acrylic (Selectaplus, Dentsply, DeTrey GmbH, Dreieich, Germany).

2.5.2. Video-EEG recordings

Continuous video-EEG monitoring was started at 10 months after TBI for 3 weeks to detect the occurrence of spontaneous seizures. Immediately after the electrode implantation rats were placed in Plexiglas cages (47 × 29 × 50 cm, one rat per cage). EEG was recorded in freely moving animals (2048 Hz sampling rate) using the Nervus EEG Recording System connected with a Nervus Magnus 32/8 Amplifier (Taugagreining, Iceland), and filtered (high-pass filter 0.3 Hz cut-off, low-pass 1000 Hz). The behavior of the animal was recorded using a WV-BP330/GE Video Camera (Panasonic, wide angle-lens) that was positioned above the cages and connected with a SVT-N72P Time Lapse VCR (Sony) and a PVM-145E Video Monitor (Sony). A type WFL-II/LED15W infrared light (Videor Technical, GmbH, Germany) was used at night to allow continuous 24 h/d video-monitoring.

2.5.3. Video-EEG analysis

Seizure occurrence was detected by using a seizure detection algorithm and confirmed by visual analysis (Andrade et al., 2018). A spontaneous electroencephalographic seizure was defined as a high-amplitude rhythmic discharge that clearly represented an atypical EEG pattern (i.e., repetitive spikes, spike-wave discharges, poly-spike-and-wave, or slow-waves, frequency and amplitude modulation) that lasted > 10 s (Fig. 2C). If an electrographic seizure was observed, its behavioral severity was assessed from the corresponding video recording according to a modified Racine scale (Racine, 1972): Score 0, electrographic seizure without any detectable motor manifestation; Score 1, mouth and face clonus, head nodding; Score 2, clonic jerks of a forelimb; Score 3, bilateral forelimb clonus; Score 4, forelimb clonus and rearing; and Score 5, forelimb clonus with rearing and falling. As described previously by Rodgers et al. (2015), we also noted the occurrence of spike-wave discharges in both the sham-operated and injured rats, but they were not counted as TBI-related seizures (Fig. 2D). The EEGs were also analyzed for automatic detection of seizures using an algorithm developed in-house in Spike2 (ver.9) scripting language (see Andrade et al., 2018). A rat was diagnosed with PTE if it had at least one unprovoked spontaneous electrographic seizure in the EEG.

2.6. Pentyleneterazole seizure-susceptibility test

To determine whether seizure susceptibility was increased, rats were injected with a subconvulsant dose of pentylenetetrazole (PTZ, 1,5-pentamethylenetetrazole, 98%, Sigma-Aldrich YA-Kemia Oy, Finland) dissolved in sterile 0.9% saline (25 mg/kg, 18 mg/ml, 1.39 ml/kg, i.p.) at 11 months post-TBI. Following the PTZ injection, rats were placed into transparent plexiglas cages (47 × 29 × 50 cm, one rat per cage) and video-EEG was recorded for 60 min after PTZ administration.

A PTZ-induced electrographic seizure was defined as a > 5 s duration high-amplitude rhythmic discharge with a clear onset, temporal evolution in wave morphology and amplitude, and offset (Fig. 2E). A spike was defined as a high-amplitude (twice the baseline) sharply contoured waveform with a duration of 20–70 milliseconds. Latency to the first spike and the total number of spikes were calculated during 60 min after PTZ administration. Spike counting did not include the electrographic seizure events. Rats with a latency to the fist PTZ-induced spike less than -1SD of the control mean were considered epileptogenic (Nissinen et al., 2017). In addition to continuous video recording, behavior of the animal was monitored by an observer. The time of the occurrence of epileptiform behavioral events was recorded and scored according to a Racine scale (1 = behavioral symtoms, 1: head nodding, chewing, sniffing; 2 = myoclonic jerks of one forelimb; 3 = bilateral forelimb clonus; 4 = forelimb clonus with rearing; 5 = tonic–clonic convulsion).

2.7. Histology and immunohistochemistry

2.7.1. Assessing BBB leakage using fluorescein

Rats were injected at 1 week after the PTZ test with a BBB tracer, fluorescein (FSC; 100 mg/kg, 50 mg/ml, via the tail vein, Merck, Darmstadt, Germany) under isoflurane anesthesia (1–2 vol%) as described previously (Van Vliet et al., 2007). At 2.5 h after tracer injection, rats were deeply anesthetized with an intraperitoneal injection of sodium pentobarbital (58 mg/kg) and chloral hydrate (60 mg/kg), and

intracardially perfused according to the Timm fixation protocol (Kharatishvili et al., 2007). The brains were removed, cryoprotected in 20% glycerol in 0.02 M potassium phosphate buffer, pH 7.4, for 24 h, frozen in dry ice, and stored at −70 °C. A one-in-five series of frozen sections were cut at 30-μm thickness in the coronal plane throughout the brain using a sliding microtome. Sections were collected into tissue collection solution (30% ethylene glycol, 25% glycerol in 0.05 M sodium phosphate buffer) and stored at −20 °C until processed. To detect extravasation of FSC, sections were mounted on slides (Superfrost Plus, Menzel, Braunschweig, Germany) and coverslipped with mounting medium for fluorescence (Vectashield, Vector Laboratories, Burlingame, CA, USA) containing 4′,6-diamidino-2-phenylindole (DAPI). FSC was detected using a confocal-laser scanning microscope (Zeiss LSM510; excitation 488 nm, emission 520 nm). Images were made using Zeiss software (Zeiss LSM Image browser). The extent of FSC extravasation was quantified in the perilesional cortex, lateral thalamus, and hippocampus. The confocal grid (271 × 271 μm; 15 × 15 squares) was positioned over the selected brain region, the number of squares that contained a FSC signal was counted, and the intensity of the FSC staining was measured using the histogram function in Adobe Photoshop CS5 (version 12.0). A 'permeability index' (number of squares that contained a FSC signal x FSC intensity) was constructed as described previously (Van Vliet et al., 2007). FSC data were compared with gadobutrol data obtained with MRI (Gd-leakage).

2.7.2. Immunohistochemical staining of BBB leakage

In addition to fluorescein analysis, IgG was detected using immunohistochemistry to visualize BBB leakage. Briefly, coronal sections were collected from the tissue collecting solution. After washing in 0.02 M potassium phosphate-buffered saline (KPBS), the sections were incubated in 1% H_2O_2 to inactivate endogenous peroxidase, and then, blocked as described in the next paragraph. Then, the sections were incubated for 2 h at room temperature (RT) with a rabbit antibody against rat IgG (1:300; BA-4000; Vector laboratories) in 1% normal horse serum and 0.4% Triton X-100 in KPBS. After washing three times with 0.02 M KPBS (10 min each), they were incubated in an avidin-biotin solution (1:200, PK-4000; Vector Laboratories) made in KPBS for 1 h at RT. The sections were washed in 0.02 M KPBS, and subsequently, incubated with the secondary antibody solution, followed by the avidin-biotin solution. The IgG staining was visualized using 0.05% 3,3′-diaminobenzidine.

2.7.3. Immunohistochemical staining of blood vessels, macrophages, microglial cells, and reactive astrocytes

To visualize blood vessels, inflammation, and glial reactivity, sections were stained with antibodies against rat endothelial cell antigen-1 (RECA-1), CD68 (activated macrophage/monocyte/microglia marker), OX-42 (microglial marker), or vimentin (reactive astrocyte marker), respectively. Briefly, 3 consecutive coronal sections (3.5–4.1 mm posterior to bregma, 300 μm apart from each other) were collected from tissue collecting solution. After three washes (10 min each) in 0.02 M potassium phosphate-buffered saline (KPBS; pH 7.4), the sections were incubated in 1% H_2O_2 solution for 15 min to remove endogenous peroxidase. After rinsing 6 times with KPBS (5 min each), non-specific binding was blocked by incubating the sections for 2 h at RT in a solution containing 10% normal horse serum (NHS) and 0.4% Triton X-100 prepared in KPBS. Next, the sections were incubated overnight at 4 °C with either mouse anti-rat RECA-1 (1:5000; MCA970R, AbD Serotec), mouse-anti rat CD68 (1:2000; MAB1435, Millipore), mouse anti-rat OX-42 (1:4000; MCA275G, AbD Serotec), or mouse anti-rat vimentin (1:2000; M0725, DAKO) in a solution containing 1% NHS and 0.4% Triton X-100 made in 0.02 M KPBS. Then, sections were washed with KPBS (3 times, 10 min) and incubated for 2 h at RT in a secondary antibody solution, containing biotinylated horse anti-mouse IgG (1:200; BA-2000; Vector laboratories), 1% NHS, and 0.4% Triton X-100 in KPBS. Subsequently, the sections were washed with KPBS (3 times, 10 min each) and incubated in an avidin-biotin solution (1:200, PK-4000; Vector Laboratories) made in KPBS for 1 h at RT. After washing in KPBS, sections were incubated in recycled secondary antibody solution for 45 min, and then in avidin-biotin solution for 30 min. The secondary antibody was visualized with 0.05% 3,3′-diaminobenzidine (Pierce Chemical) and 0.04% H_2O_2 in KPBS. Finally, the sections were washed with 0.1 M PB, and mounted on gelatin-coated slides. The staining was intensified with osmium tetraoxide (Electron Microscopy Sciences, Hatfield, PA, USA) and thiocarbohydrazide (Electron Microscopy Sciences, Hatfield, PA, USA)(Lewis et al., 1986). Sections were coverslipped with Depex.

2.7.4. Quantification of RECA-1, CD68, OX-42 and vimentin immunohistochemistry

The intensity of RECA-1, CD68, OX-42 and vimentin immunoreactivity was quantified using NIH ImageJ software (version 1.47v). The analysis was performed in the perilesional cortex, ipsilateral hippocampus, and ipsilateral thalamus. Briefly, digital photomicrographs were captured using Zeiss Axio Imager 2 microscope equipped with a Zeiss axiocam 506 colour camera (Carl Zeiss, Germany). The images were uploaded to the ImageJ software, and the region of interest (ROI) (perilesional cortex, hippocampus, thalamus) was outlined (ROI matched the ROIs outline in MR images in Fig. 1). The images were converted to an 8-bit grayscale image and thresholded (*i.e,* pixels within the grayscale range of the staining were segmented, i.e. 0–255). The area and the area fraction (i.e., the area of staining divided by the area of ROI) of RECA-1, CD68, OX-42 and vimentin immunoreactivities were calculated.

2.7.5. Alizarin red staining

To visual calcium deposits in the brain tissue, sections were stained with 2% alizarin red S solution (A5533-25G, Sigma-Aldrich, St Louis, MO, USA). Briefly, sections mounted on gelatin-coated slides were rehydrated through a descending series of ethanol, rapidly rinsed in distilled water and then dipped into 2% alizarin red S solution for 30 s. The slides where subsequently dipped (20 times) in acetone, then into an acetone-xylene solution, cleared in xylene, and mounted using Depex.

2.7.6. Thionin staining

In order to visualize the cytoarchitectonic boundaries, neurodegeneration and lesion location, the first of the 1-in-10 series of sections (stored in 10% formalin) was stained with thionin, cleared in xylene, and cover-slipped using Depex (BDH Chemicals, Poole, UK).

2.8. Human autopsy tissue

The subjects included in this study was selected from the database of the Department of (Neuro)Pathology of the Amsterdam UMC, University of Amsterdam. Informed consent was obtained for the use of brain tissue and to access to medical records for research purposes. Tissue was obtained and used in a manner compliant with the Declaration of Helsinki and the Amsterdam UMC Research Code provided by the Medical Ethics Committee of the Amsterdam UMC. Brain samples were selected from 10 individuals (3 females and 7 males; age range 32–80 years) who died from TBI (without evidence of neurodegenerative changes or a clinical history of cognitive impairment). The causes of injury included a car accident, falls, a kick from a horse in the face, and a hit by an explosive device. For the majority of cases TBI was severe and the lesion was located in the cortex. Post-TBI survival time was 24 h in three, 1 week in three, 1 month in one, 6 months in one, and 38 years or more in two cases (38 and 54 years). None of the patients had acute post-traumatic seizures. The three patients with a survival time of 6 months, 38 years and 54 years had PTE, with a latency of respectively 6 months, 1 year and 1 year.

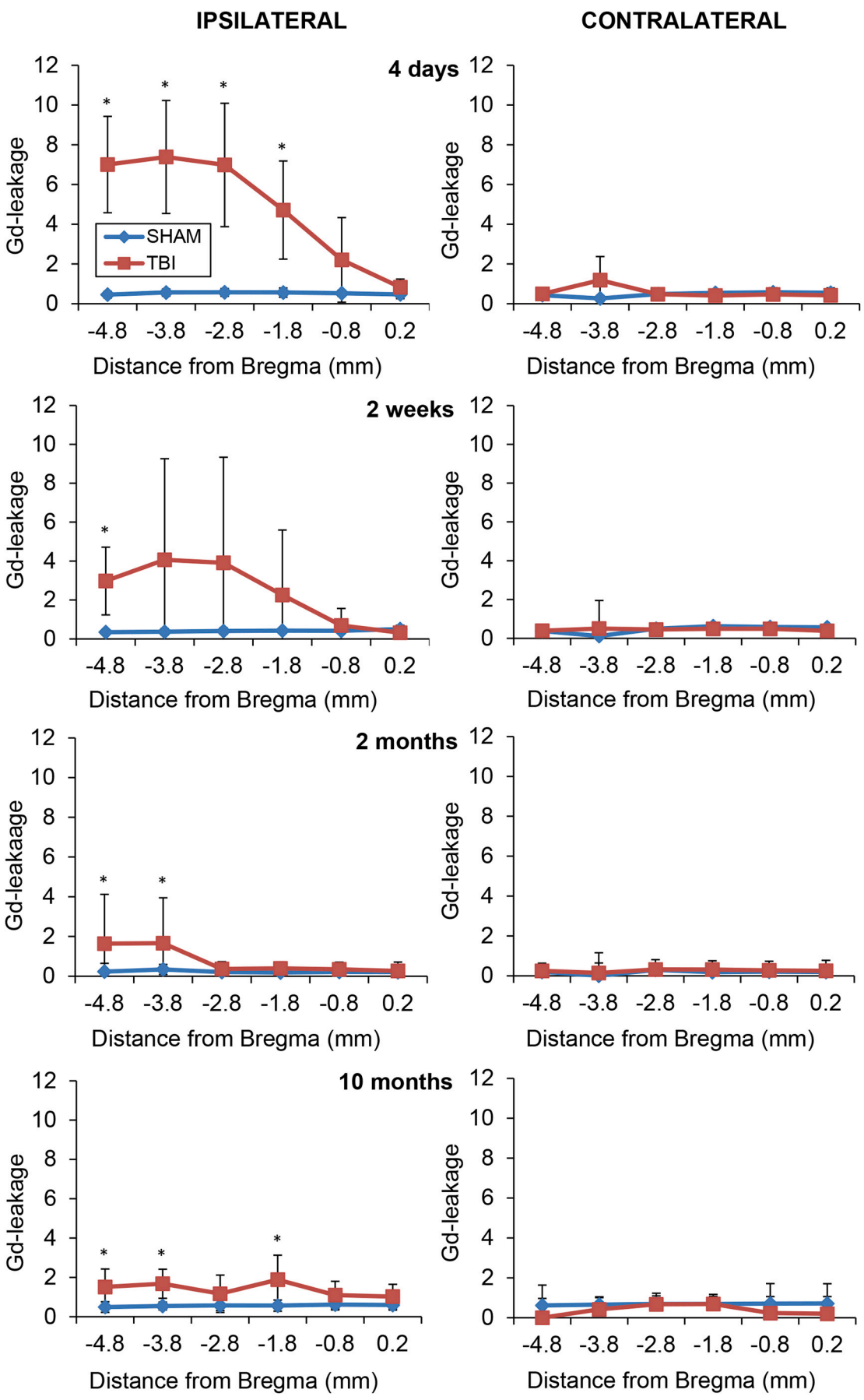

(caption on next page)

Fig. 4. Quantification of gadobutrol (Gd)-leakage in the perilesional cortex and thalamus. Line-drawings showing the Gd-leakage (y-axis) at different follow-up points. Panels on the left: In the dorsal perilesional cortex, Gd-leakage was most evident at 4 days after TBI, extending over a 4-mm rostro-caudal axis of the cortex. Gd-leakage was also detected at 2 weeks after TBI, even though to the lesser extent as compared to that at 4 days post-TBI. Some perilesional Gd-leakage was still evident at 2 and 10 months post-TBI, and in 10/12 cases it still extended over the 4-mm rostro-caudal extent. Panels on the right: Gd-leakage was also present in the lateral aspect of the ipsilateral thalamus, but not before 2 months post-TBI. Gd-leakage in the contralateral hemisphere was not different between sham-operated and injured rats, even though at 2 months post-TBI some of the injured animals showed bilateral thalamic BBB leakage. Data are shown as mean ± standard deviation. Statistical difference: *, $p < 0.05$ (Kruskall Wallis, followed by Mann-Whitney *U* test as compared to sham-operated controls).

2.8.1. Tissue preparation

Representative formalin-fixed paraffin blocks (corresponding to the site of cortical injury or located in proximity of the injured cortex, as well as the thalamus of a subset of patients (PTE, $n = 3$; survival times 6 months, 38 years and 54 years) were sectioned at 6 μm and mounted on pre-coated glass slides (Star Frost, Waldemar Knittel GmbH, Braunschweig, Germany). Sections of all specimens were processed for hematoxylin-eosin, Luxol fast blue, Nissl, Perls' stain (for Fe^{3+}), Alizarin red (for calcium), and immunohistochemical markers.

2.8.2. Immunohistochemistry

Albumin (polyclonal rabbit anti-human, DAKO, Glostrup, Denmark; 1:20000), vimentin (mouse clone V9, DAKO, Glostrup, Denmark; 1:400), human leukocyte antigen (HLA)-DP, DQ, DR (major histocompatibility complex class II, MHC-II; mouse clone CR3/43, DAKO, Glostrup, Denmark; 1:400), and CD68 (mouse clone PG-M1, DAKO, Glostrup, Denmark; 1:200) were used.

2.9. Statistical analysis

Data were analyzed using SPSS for Windows (version 22.0). The Kruskal-Wallis analysis was used to assess the difference between the sham-operated and TBI groups. If statistical significance was found, post hoc analysis was done using Mann-Whitney *U* test. Spearman rank correlation test was used to assess the correlation between Gd-leakage, FSC leakage, epileptiform activity as well as the coverage with the RECA-1, CD68, OX42, and vimentin immunoreactivities. A *p*-value less than 0.05 was considered significant. Data that were not normally distributed are reported as median and range, while data that were normally distributed are reported as mean and standard deviation.

3. Results

3.1. Impact severity, occurrence of acute post-impact seizure-like behavior, duration of apnea, and acute mortality

The mean impact severity was 3.00 ± 0.03 atm. Post-impact seizure-like behavior occurred in 31% (5/16) of rats. The duration of post-impact apnea was 17.2 ± 3.7 s (median 15 s, range 5–30 s). Four of 16 injured rats (25%) died within 48 h post-TBI, which is in line with a previous study with similar impact severity (Kharatishvili et al., 2006). The cause of death was considered to be related to TBI.

3.2. Blood-brain barrier leakage in contrast-enhanced MRI and histology

3.2.1. Contrast-enhanced MRI

At 4 days post-TBI, Gd-leakage was most evident in the dorsal perilesional cortex. Its rostrocaudal extent was 4 mm and mediolateral extent about 2 mm (Figs. 3–4). At 2 weeks post-TBI, Gd-leakage was still prominent in the dorsal perilesional cortex, even though to a lesser magnitude as compared to 4 days post-TBI. At 2 and 10 months post-TBI, Gd-leakage was still present in the dorsal perilesional cortex, extending 4 mm rostrocaudally and 1–2 mm mediolaterally (Figs. 3–4). Interestingly, Gd-leakage was not detected in the ventral perilesional cortex at any time point.

Gd-leakage became evident also in the lateral aspect of the ipsilateral thalamus, but not earlier than 2 months post-TBI (Figs. 3–5). Gd-leakage was not detected at any timepoint in the more medial aspects of the ipsilateral thalamus, hippocampus, amygdala, piriform cortex, or entorhinal cortex in rats with TBI (Figs. 3 and 5; **Supplementary Fig. 1**).

3.2.2. Correlation between Gd and FSC leakage

Gd-leakage in MRI slices at 10 months post-TBI was compared to post-mortem presence of FSC (a tracer to detect BBB leakage) in histological sections from the same rats at 11 months post-TBI. Like Gd-leakage, the FSC permeability index was increased in the dorsal perilesional cortex and the lateral aspects of the ipsilateral thalamus in rats with TBI as compared to that in sham-operated rats (Fig. 6). FSC leakage was not observed in any other ROI (e.g., septal hippocampus, see Fig. 6F, G), confirming the MRI data. Furthermore, the higher the Gd-leakage in MRI in the dorsal perilesional cortex or lateral thalamus in TBI rats, the higher the FSC permeability index in the same animals (Fig. 6H: $r = 0.72$, $p < 0.05$; Fig. 6I: $r = 0.75$, $p < 0.05$, respectively).

3.2.3. Vascular remodeling in the cortex, thalamus, and hippocampus in histological sections at 11 months post-TBI

RECA-1 immunostaining at 11 months post-TBI revealed no changes in morphology or orientation of blood vessels in the contralateral cortex, hippocampus, or thalamus as compared to sham-operated controls (Fig. 7A–D). Therefore, the following description focuses on the ipsilateral hemisphere.

3.2.4. Lesion core and perilesional cortex

RECA-1 immunostaining indicated a conspicuous absence of blood vessels within the lesion core at 11 months post-TBI (Fig. 7E). In some animals with TBI, we found RECA-1 positive vascular sprouts in the lesion core (insert in Fig. 7E). In the perilesional cortex, blood vessels did not differ morphologically from that in control rats but their orientation appeared often parallel to the cortical surface (Fig. 7E) as opposed to a non-specific orientation in sham-operated controls (Fig. 7A). Quantitative analysis revealed that the area fraction of RECA-1-immunoreactive blood vessels [i.e., the fraction (%) of the ROI covered by RECA-1 immunoreactivity] did not differ between TBI and sham-operated controls [TBI median 27.5% (range 15.7–34.9) vs. sham median 23.4% (range 19.2–27.6), $p > 0.05$] (Fig. $8A_1$).

3.2.5. Ipsilateral thalamus

Visual analysis revealed a higher density of tortuous blood vessels, particularly in the ventroposterior medial (VPM) and ventroposterior lateral (VPL) nuclei (Fig. 7C, G). Quantitative analysis showed that the area fraction of RECA-1-immunoreactive blood vessels was, however, comparable between TBI and sham-operated controls [TBI median 17.3% (range 9.7–22.1) vs. sham median 21.1% (range 13.3–29.3), $p > 0.05$] (Fig. $8C_1$).

3.2.6. Ipsilateral hippocampus

The vascular orientation and morphology of animals with TBI were comparable to that in sham-operated controls (Fig. 7B, F). Quantitative analysis revealed that RECA-1 immunoreactivity did not differ between TBI and sham-operated controls [TBI median 9.8% (range 7.5–15.4) vs. Sham median 17.3% (range 5.8–21.5), $p > 0.05$] (Fig. $8B_1$).

In addition, we observed a higher density of RECA-1-

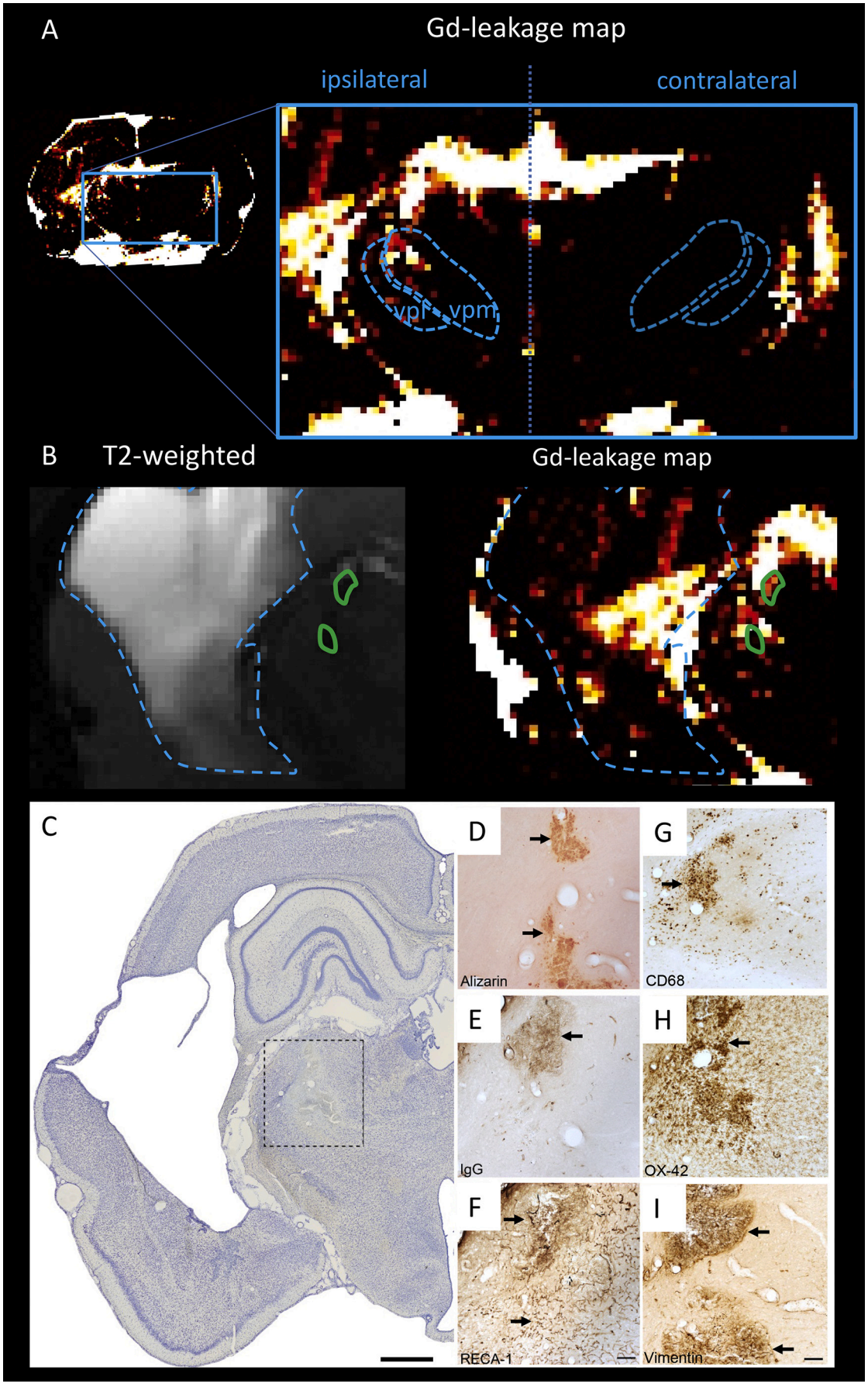

(caption on next page)

Fig. 5. Blood-brain-barrier (BBB) dysfunction and inflammation in the lateral thalamus. (A) The gadobutrol (Gd)-leakage map revealed BBB dysfunction in the thalamus, specifically in the ipsilateral ventroposterior medial (vpm) and ventroposterior lateral (vpl) nuclei (rat #e25). (B) Higher magnification images demonstrating prominent Gd-leakage (red/yellow colors in Gd-leakage map) from the blood vessels around the T2-negative calcifications (black spots on T2-weighted images, the borders are indicated with green lines). (C) A coronal thionin-stained section from the level of lesion core in a rat 11 months post injury (rat #e25) presented in A and B. The dotted rectangle indicates part of the lateral thalamus which is shown in D-I. Calcifications, BBB leakage and associated chronic inflammation were confirmed by histological analysis using (D) alizarin (calcifications), (E) IgG (BBB leakage), and (F) RECA-1 stainings (blood vessels). Furthermore, RECA-1 positive blood vessels were surrounded by a zone with increased expression of (G) CD68 (activated macrophages/monocytes/microglia), (H) OX-42 (microglia), and (I) vimentin (astrocytes; arrows in G-I). Scale bar equals 1 mm in panel C and 100 μm in panels F and I. Abbreviations: FSC = fluorescein, Gd = gadolinium, PTE = post-traumatic epilepsy, TBI = traumatic brain injury. (For interpretation of the references to colour in this figure legend, the reader is referred to the web version of this article.)

immunoreactive blood vessels in the white matter structures such as the corpus callosum in rats with TBI as compared to sham-operated controls (arrows in Fig. 7H).

3.3. Increased expression of inflammatory markers in histological sections at 11 months post-TB

3.3.1. Macrophage/monocyte/microglia activation

An antibody raised against CD68 was used to detect activated macrophages/monocytes/microglia. The presence of CD68-positive cells was extremely rare in sham-operated controls in the cortex, hippocampus or thalamus **(**Fig. 7I–L**)**.

After TBI, CD68 immunoreactivity was very low in all the areas analyzed contralaterally. However, in the ipsilateral hemisphere, strong CD68 immunoreactivity was observed around the lesion core and in layer VI of the perilesional cortex **(**Fig. 7M**)**. The highest density of intensely labeled CD68-immunoreactive cells was observed in the ipsilateral thalamus, particularly in the ventral posteromedial (VPM) and ventral posterolateral (VPL) nuclei **(**Figs. 5H and 7O**)**. The very few CD68-immunoreactive cells detected in the ipsilateral hippocampus were typically located in the dentate gyrus **(**Fig. 7N**)**.

Quantitative analysis confirmed higher CD68 immunoreactivity [i.e., the fraction (%) of the ROI covered by CD68 immunoreactivity] ipsilaterally in the lesioned cortex of rats with TBI [median 2.9% (range 1.2–4.2) vs. median 0.05% (range 0.02–0.4), $p < 0.01$ as compared to sham-operated controls, Fig. 8 A_2], thalamus [median 2.8% (range 1.9–3.7) vs. median 0.2% (range 0.1–0.4), $p < 0.01$, Fig. 8C_2] and hippocampus [median 0.6% (range 0.5–0.8) vs. median 0.2% (range 0.1–0.6), $p < 0.05$, Fig. 8B_2]. Moreover, CD68 immunoreactivity was also observed bilaterally in the corpus callosum in rats with TBI but was totally absent in sham-operated controls **(**Fig. 7L, P**)**.

3.3.2. Astrocyte activation

An antibody against vimentin was used to visualize blood vessels and activated astrocytes. In control animals, vimentin immunoreactivity was mainly expressed in blood vessels in the cortex, thalamus, and hippocampus **(**Fig. 9A–D**)**.

After TBI, vimentin immunoreactivity in the contralateral hemisphere was similar to that in sham-operated controls. Ipsilaterally, strong vimentin immunoreactivity was detected within and around the lesion core in the perilesional cortex **(**Fig. 9E**)**. In the ipsilateral thalamus, vimentin immunoreactivity was much stronger in astrocytes as compared to blood vessels. Furthermore, clusters of vimentin-immunoreactive astrocytes were observed in the VPM and VPL nuclei (Figs. 5I and 9G). In the ipsilateral hippocampus, vimentin immunoreactivity was typically expressed in blood vessels and the intensity was comparable to that in controls **(**Fig. 9F**)**.

In white matter bundles such as the corpus callosum, there was a prominent bilateral astrocytic vimentin immunoreactivity both in injured and control animals. However, the intensity of the immunoreactivity was stronger in rats with TBI as compared to sham-operated controls **(**Fig. 9H**)**. Quantitative analysis of the area fraction of vimentin immunoreactivity in the different ipsilateral brain areas showed higher reactivity in rats with TBI as compared to sham-operated controls in the perilesional cortex (median 5.9% (range 4.6–9.2) vs. median 1.0% (range 0.8–2.4), $p < 0.01$, Fig. 8A_4] and thalamus [median 11.5% (range 5.9–12.7) vs. median 2.0% (range 0.7–6.4), $p < 0.05$, Fig. 8C_4], but not in the hippocampus [median 3.3% (range 2.1–6.7) vs. median 2.3% (range 0.8–5.9) $p > 0.05$, Fig. 8B_4].

3.3.3. Microglial reactivity

To specifically evaluate microglial reactivity, sections were stained with an antibody against CD11b/c (OX-42), a marker for microglial cells. In sham-operated controls, low immunoreactivity was observed bilaterally in the cortex, thalamus, and hippocampus **(**Fig. 9I–L**)**.

In rats with TBI, the intensity of OX-42 immunoreactivity in the contralateral hemisphere was similar to sham-operated controls in all areas analyzed. However, strong ipsilateral OX-42 immunoreactivity was observed in the lesion core and in the perilesional cortex **(**Fig. 9M**)**. Quantitative analysis confirmed higher OX-42 immunoreactivity in the perilesional cortex of rats with TBI [median 10.8% (range 7.0–14.2) vs. median 1.3% (range 0.6–1.8), $p < 0.01$ as compared to sham-operated controls, Fig. 8A_3].

Similarly, in the ipsilateral thalamus, there was a strong OX-42 immunoreactivity in microglial cells in rats with TBI as compared to sham-operated controls **(**Figs. 5H and 9O**)**. Clusters of OX-42 immunoreactive glial cells were observed in the thalamic VPM and VPL nuclei. In correspondence with visual analysis, the area fraction of OX-42 immunoreactivity in the ipsilateral thalamus was higher in rats with TBI [median 14.8% (range 8.3–20.3) vs. median 2.5% (range 1.6–7.1), $p < 0.01$ as compared to sham-operated controls, Fig. 8C_3].

In the ipsilateral hippocampus of rats with TBI, the intensity and the distribution of microglial OX-42 immunoreactivity was comparable to that in sham-operated controls **(**Fig. 9N**)**. This was confirmed quantitatively as the area fraction of OX-42 immunoreactivity in the ipsilateral hippocampus did not differ between TBI and controls animals [median 10.7% (range 4.7–18.6) vs. median 2.7% (range 1.2–10.9), $p > 0.05$, Fig. 8B_3].

3.3.4. Gd-leakage in relation to histology

In the perilesional cortex at 11 months post-injury, the higher the Gd-leakage, the higher the RECA-1 expression in blood vessels ($r = 0.734$, $p < 0.01$, Fig. 8D_1) and larger the area occupied by CD68-positive macrophages/monocytes/microglia ($r = 0.699$, $p < 0.05$, Fig. 8D_2).

Interestingly, Gd-leakage and IgG-immunoreactivity in the lateral thalamus were specifically evident in the areas with tortuous blood vessels surrounding T2-negative calcifications **(**Fig. 5B**)**, which was confirmed by histological analysis using alizarin and RECA-1 stainings **(**Fig. 5D–F**)**. Furthermore, these tortuous blood vessels were surrounded by a zone with increased expression of CD68, OX-42 and vimentin Fig. 5G–I**)**.

3.3.5. Occurrence of unprovoked seizures and increase in seizure susceptibility - relation to BBB permeability and inflammatory response

Duration of video-EEG monitoring was 27–28 days in 15 (10 TBI, 5 sham) and 10 days in 3 (2 TBI, 1 sham) rats. Only 1 (#e16) of 12 rats (8%) with TBI showed unprovoked late seizures during the continuous video-EEG recording preceding the PTZ test. The rat had three seizures which occurred on the 11th, 19th, and 20th day after initiation of the

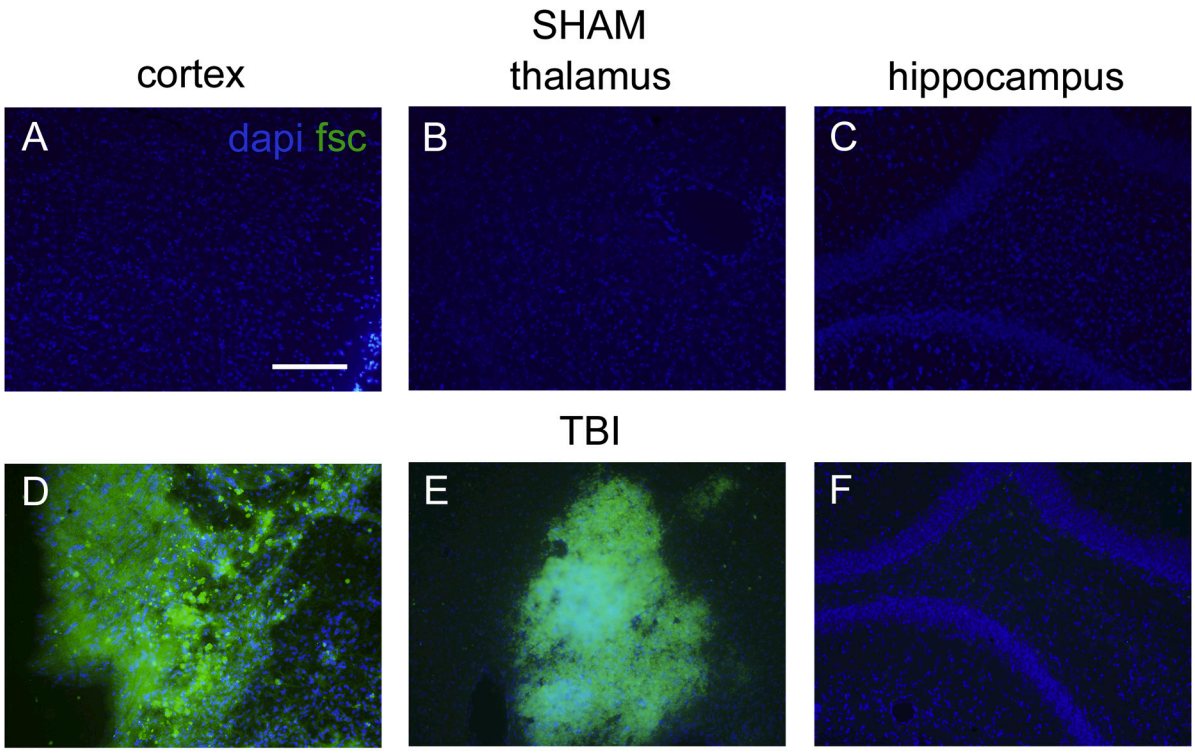

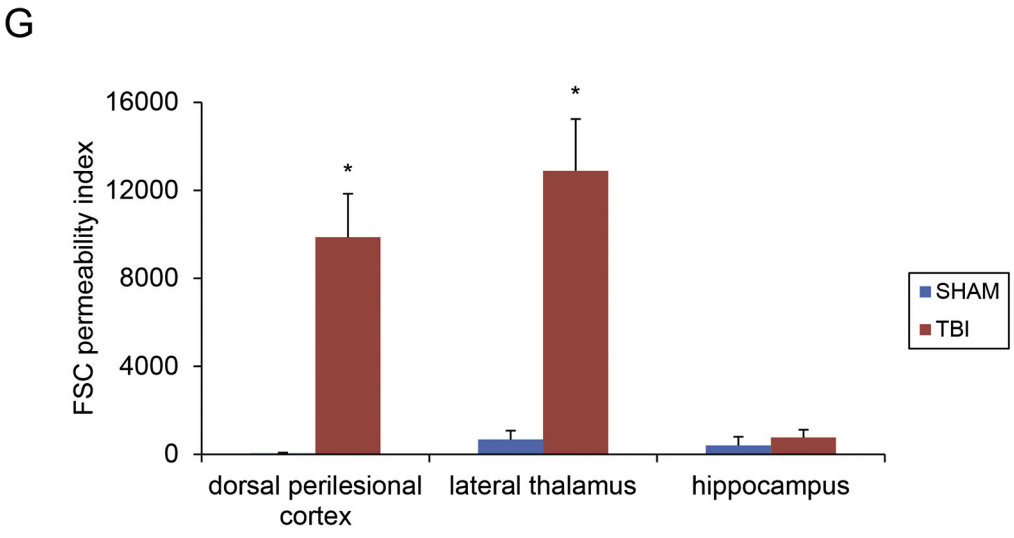

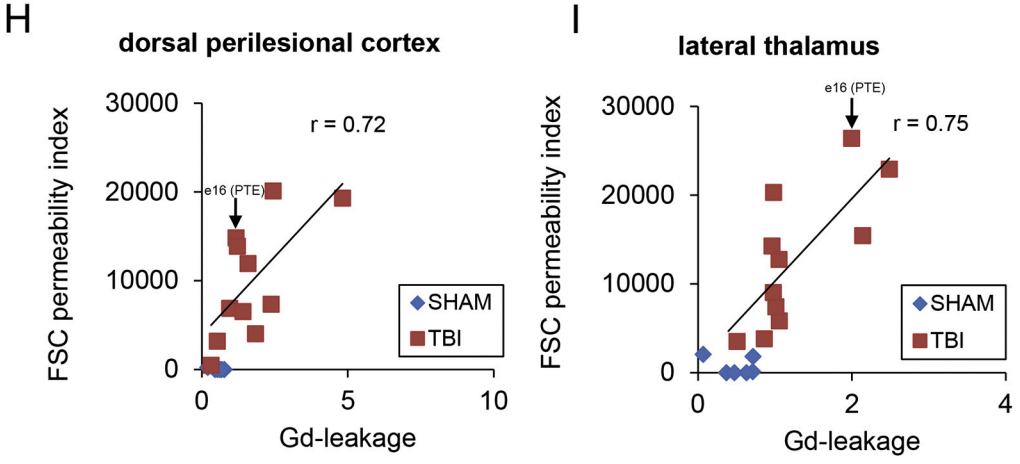

(caption on next page)

Fig. 6. Correlation between gadobutrol and fluorescein leakage. (A-F) Photomicrographs from fluorescein (FSC, green) labeled sections were used for microscopic quantification of blood-brain-barrier (BBB) leakage at 11 months post-TBI. 4′,6-diamidino-2-phenylindole (DAPI, blue) was used as nuclear counterstaining. Data from histological analysis were compared with MRI-based BBB leakage measurements using the contrast agent gadobutrol (Gd) in the same rats, which were performed at 10 months post-TBI. (G) The FSC permeability index (number of squares of the confocal grid that contained a FSC signal x FSC intensity) was increased in the dorsal perilesional cortex (see panel D) and lateral thalamus (see panel E) in rats with TBI as compared to sham-operated controls (panels A and B). FSC leakage was not detected in any of the other ROIs (i.e., septal hippocampus, F and G), confirming MRI data. Furthermore, the higher the FSC permeability index, the greater the Gd-leakage in MRI in the (H) dorsal perilesional cortex $r = 0.72, p < 0.05$) and (I) ipsilateral lateral thalamus ($r = 0.75$, $p < 0.05$) after TBI. Arrow indicates the rat (#e16) with post-traumatic epilepsy (PTE; unprovoked seizures). (For interpretation of the references to colour in this figure legend, the reader is referred to the web version of this article.)

recording. All three seizures occurred at transition from N3 to REM sleep, lasted for 208, 91 and 69 s, respectively, and were convulsive. A typical example of a spontaneous seizure is shown in Fig. 2C. Both sham-operated control rats as well as TBI rats showed spike-wave discharges during wakefulness, which were not counted as TBI-induced seizures **(**Fig. 2D**).**

Seizure susceptibility was assessed using the PTZ-test at 11 months post-TBI. Four of 6 (75%) sham-operated (mean duration 47 ± 20 s, range 28–74 s) and 5 of 12 (42%) TBI rats (72 ± 34 s, range 33–122 s showed 1–2 PTZ-induced seizures, Fig. 2E)($p > 0.05$, χ^2).

The latency to the first PTZ-induced spike in the sham-operated controls was 169 ± 56 s (median 159 s, range 101–252 s) and in the TBI group 127 ± 86 s (median 109 s, range 19–328 s)($p > 0.05$) **(**Fig. 10A**).** The large variability in the TBI group suggested variability in seizure susceptibility. Consequently, 7 of the 12 TBI rats (58%) with latency to the first spike less than 113 s (less than -1SD of the control mean) were considered epileptogenic (closed circles in Fig. 10A), including rat #e16 that had a late spontaneous seizure.

The total number of PTZ-induced spikes during the 60-min post-injection follow-up was 641 ± 348 (median 597, range 230–1054) in sham-operated controls and 1448 ± 828 (median 1093, range 482–2812) in the TBI group ($p < 0.05$, Fig. 10B).

3.3.6. Seizure susceptibility and BBB dysfunction

Even though Gd-leakage was elevated both in the perilesional cortex and thalamus at 10 months post-TBI, there was no difference in the mean Gd-leakage between rats with or without increased seizure susceptibility **(**Fig. 10C–D**).** Also, there was no correlation between the Gd-leakage in the perilesional cortex or thalamus and the latency to the first spike in the PTZ-test in rats with TBI **(**Fig. 10E–F**).** Unexpectedly, the greater the total number of PTZ-induced spikes, the lower the Gd-leakage ($r = -0.745$, $p < 0.001$, Fig. 10G).

Finally, the proportional area of RECA-1 -immunoreactivity in the perilesional cortex (signaling on formation of new capillaries) was greater in rats with no increase in PTZ-induced seizure susceptibility than in rats with increased seizure susceptibility (Fig. 8A_1).

3.3.7. Seizure susceptibility and chronic neuroinflammation

We found chronically increased neuroinflammation, particularly in the perilesional cortex and ipsilateral thalamus and to a lesser extent in the ipsilateral hippocampus. However, there was no difference between the rats with normal and shortened latency to the first PTZ-induced spike except in the ipsilateral hippocampus, in which both the area of OX42 and vimentin immunoreactivities were higher in rats with increased seizure susceptibility (both $p < 0.05$, Fig. 8$B_{3–4}$). In the perilesional cortex, CD68 immunoreactivity was actually greater in rats with no-increase in seizures susceptibility as compared to those with increased seizure susceptibility ($p < 0.05$, Fig. 8A_2). Interestingly, the greater the perilesional RECA-1 immunostaining, the more prominent the CD68-positive macrophages/monocytes/microglia response (**Supplementary Fig. 2**).

3.4. Histological analysis of human tissue

Evaluation of sections from the lesioned cortex, thalamus and the corpus callosum indicated presence of both focal gray matter and white matter damage. Axonal injury was visualized by APP immunohistochemistry (data not shown). Presence of iron, hemosiderin-laden macrophages, and albumin immunoreactivity indicating BBB leakage in the cortex and to a lesser extent in the thalamus was most evident shortly after TBI, but was also evident in patients who survived longer (> 1 month up to 54 years after TBI) although to lesser extent **(**Fig. 11A–B, E–F**).** In addition, the adjacent sections showed foci of cortical and thalamic calcifications **(**Fig. 11C–D**).** Furthermore, neuroinflammation was detected in these brain regions. Microglial activation was visualized by an antibody recognizing MHC class II expression **(**Fig. 11K–L**)** and amoeboid cells by a CD68 antibody **(**Fig. 11G–H**).** Neuroinflammatory markers were present in the white and gray matter of individuals who survived at least several weeks after TBI. Furthermore, astrogliosis **(**Fig. 11I–J**)** was evident in the cerebral subcortical white matter and also to a lesser extent in the thalamus.

4. Discussion

A large number of studies have reported damage to structural components of BBB, neurovascular coupling, and cerebrovascular reactivity in experimental and human TBI, even weeks to several months after injury (for reviews, see (Salehi et al., 2017; Sandsmark et al., 2019; Shlosberg et al., 2010; van Vliet et al., 2014a). However, prospective long-term in vivo follow-up studies of BBB permeability are not available. To fill the gap, we applied Gd-MRI to investigate the spatiotemporal evolution of BBB damage over a period of 11-months after lateral FPI -induced TBI, a commonly used rat model of human closed-head injury and post-traumatic epilepsy. We also investigated association BBB leakage with neuroinflammation and epileptogenesis. Finally, we assessed human autopsy brain tissue sampled up to 54 y post-TBI to assess the translatability of experimental data. We had four major findings. First, BBB damage detected by Gd-MRI was present in the dorsal perilesional cortex and ipsilateral thalamus even for up to 12 months post-TBI. Second, severity of Gd-leakage associated with increased capillary density in the perilesional cortex. Third, it also associated with a chronic focal CD68+ and OX42+ microgliosis, being most prominent in the impacted cortex and ipsilateral thalamus. Fourth, unlike expected, chronic perilesional and thalamic Gd-leakage and neuroinflammation did not associate with increased seizure susceptibility or epilepsy after TBI. Finally, like in the animal model, we detected chronic BBB leakage, neuroinflammation, and calcifications in cortical and/or thalamic brain tissue of patients with TBI and/or PTE.

4.1. Persistent BBB dysfunction after TBI

Our study demonstrates a remarkable spatiotemporal evolution in the severity of chronic BBB impairment between the brain areas after lateral FPI -induced TBI. Like in previous MRI studies, we found robust Gd-leakage in the lesioned cortex at 4 days after TBI (Lin et al., 2012; Schneider et al., 2002). Thereafter, the cortical Gd-leakage declined, but remained elevated at 2 weeks, 2 months, and even at 10 months post-TBI as compared to that in controls. Interestingly, the higher the Gd-leakage at 10 months, the greater the density of RECA-1 positive blood vessels, suggesting a possible contribution of newly formed vessels to BBB leakage. Thus, our study expands the time window of previous observations. We also show that the BBB impairment was most

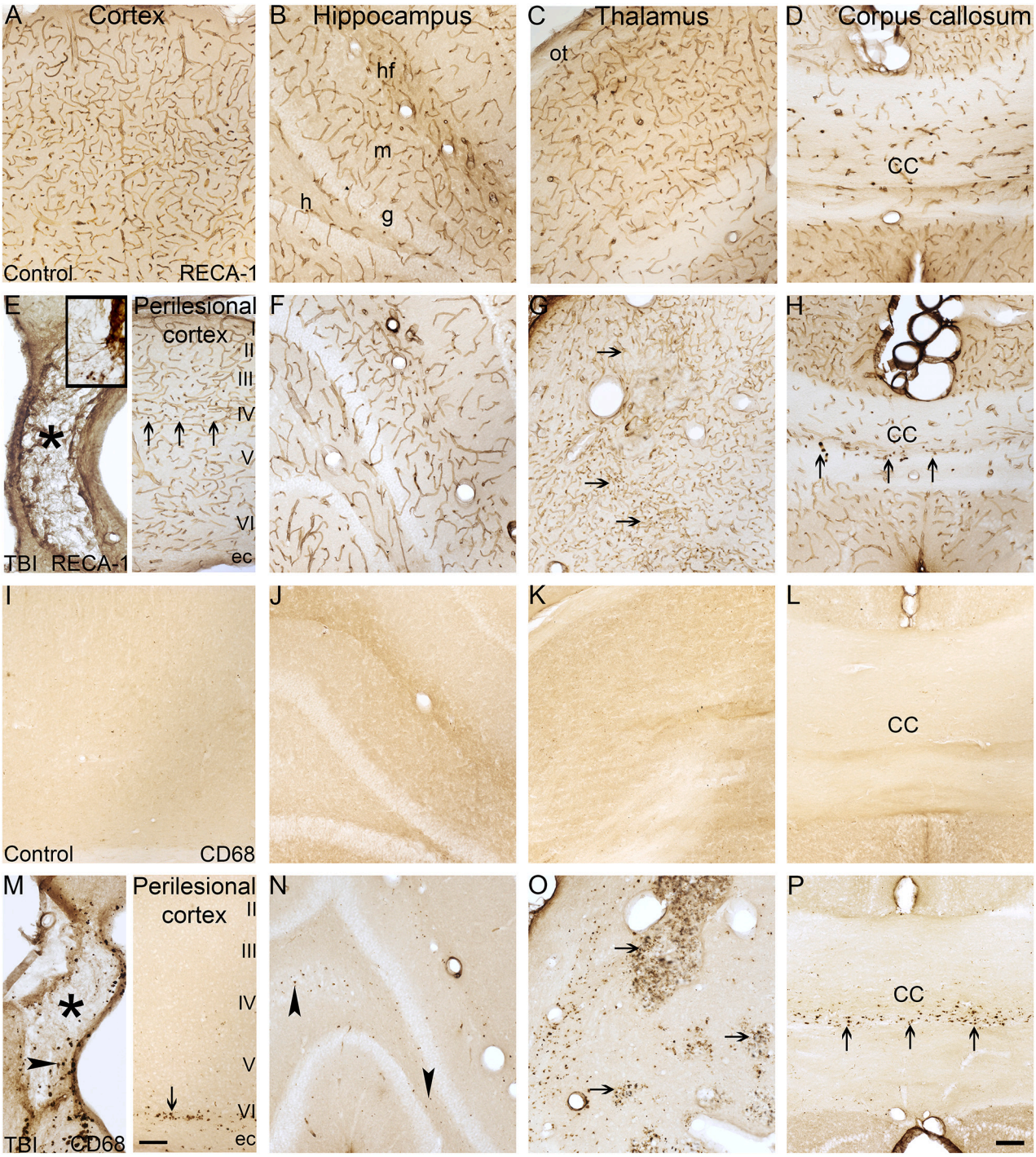

Fig. 7. Vascular and activated macrophages/monocytes/microglia staining at 11 months after traumatic brain injury (TBI). (A–D) Brightfield photomicrographs of coronal sections demonstrating the distribution of *RECA-1 immunopositive* blood vessels in the ipsilateral cortex, hippocampus, thalamus, and corpus callosum in a sham-operated control animal. (E–H) *RECA-1 immunoreactive* blood vessels in a rat with TBI. Note the vascular sprouting within the lesion (insert in panel E). The blood vessels in the perilesional cortex (panel E) appear orientated parallel to the cortical surface in layer IV (arrows). Also, note the tortuosity of the blood vessel in the thalamus (arrows in G). In the corpus callosum (H), the blood vessels had a stumpy and tortuous appearance in the mid-portion (arrows in panel H). (I–L) *CD68 immunoreactivity* in the cortex, hippocampus, thalamus and corpus callosum in a sham-injured animal. Note the absence of immunoreactive cells. (M–P) *CD68 immunoreactivity* in a rat with TBI (#e16). Note the presence of CD68-positive cells within and around the lesion (arrowhead in panel M) and also in layer VI/external capsule border (arrow, M) of the perilesional cortex. Few CD68-positive cells were observed in the hippocampus proper and dentate gyrus (arrowheads in N). In the thalamus (O), CD68-positive cells were clustered within the calcium formations (arrows). In the corpus callosum (P), CD68-positive cells were located mainly in the mid-portion (arrows), corresponding to increased vascularity (panel H). Abbreviations: cc, corpus callosum; g, granule cell layer; h, hilus; m, molecular layer; ot, optic tract; hf, hippocampal fissure. Scale bar equals 100 μm (all panels).

prominent in the dorsal and rostral aspects of the cortical lesion epicenter, particularly in the S1 cortex, most of which often appears normal in structural MRI (Yasmin et al., 2019).

The thalamus atrophies both in experimental models and in human TBI over the period of months to years (Anderson et al., 1996; Immonen et al., 2009; Ramlackhansingh et al., 2011; Shultz et al., 2013; Smith

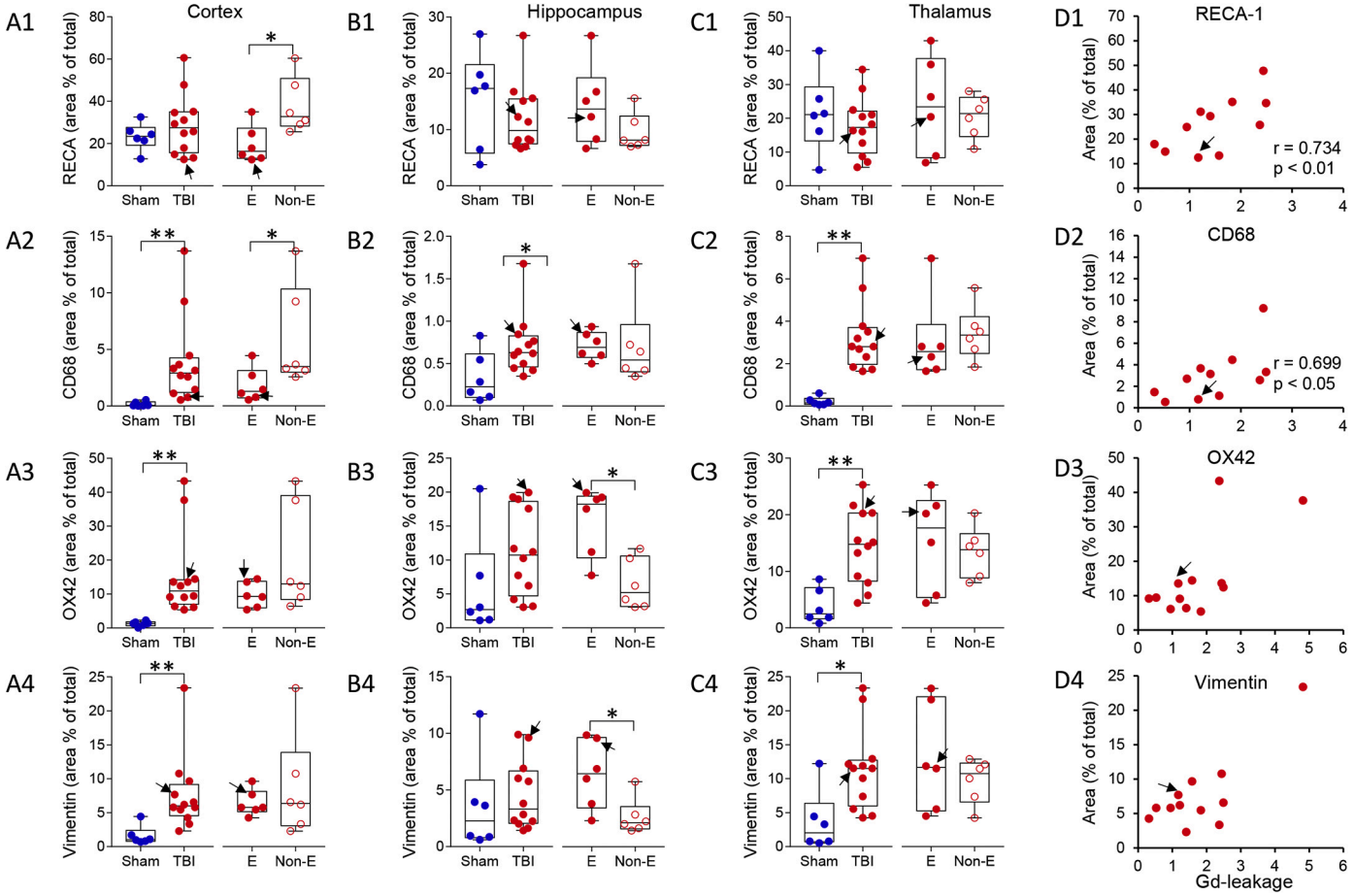

Fig. 8. Injury and epileptogenesis effects on vascular and inflammatory markers in the perilesional cortex, ipsilateral hippocampus and ipsilateral thalamus. Epileptogenesis was defined as increased susceptibility to pentyleneterazol (PTZ)-induced seizures, that is, reduced latency to the occurrence of the first epileptiform spike after PTZ injection. (A1) *In the perilesional cortex*, we did not find any injury or epileptogenesis effects on the coverage (% of the area analyzed) of RECA-1 -positive (+) vessels. (A2-A4) the coverage of CD68, OX42 and vimentin was greater in rats with TBI as compared to sham-operated controls (all $p < 0.01$). Greater coverage of CD68 did not relate with increased seizure-susceptibility. (B1-B4) *In the ipsilateral hippocampus*, no injury effect was found on hippocampal RECA-immunoreactivity. However, the coverage of CD68 ($p < 0.05$; but not OX42 or vimentin) was greater in rats with TBI as compared to sham-operated controls. Within the TBI group, coverage of OX42 and vimentin were greater in the epileptogenic (E) as compared to the non-epileptogenic (Non-E) group. (C1-C4) *In the lateral aspect of the ipsilateral thalamus*, no injury effect was not found on RECA coverage. However, the coverage of inflammatory markers was greater in the TBI group than in the sham-operated controls (CD68 and OX43 $p < 0.01$; vimentin $p < 0.05$). E and Non-E groups did not differ. (D1-D4) Correlation plots between the histological markers [% of total perilesional cortical area covered) and Gd-leakage in MRI (mean of all S1 ROIs analyzed) in the TBI group. The greater the Gd-leakage, the larger the RECA-1 or CD68 coverage. Statistical significances: * $p < 0.05$; ** $p < 0.01$; r, Spearman's rho. Arrow indicates the rat (#e16) with post-traumatic epilepsy (PTE; unprovoked seizures,).

et al., 1997; Yasmin et al., 2019). The slow evolution of thalamic BBB impairment as compared to that in the perilesional cortex adds to the evidence of slowly developing thalamic pathology in TBI. Interestingly, thalamic Gd-leakage was most prominent in the lateral aspect of the thalamus, peaking at 2 months post-TBI, remaining elevated during the entire 10-months follow-up. These thalamic areas, particularly the VPM and VPL nuclei project to the somatosensory cortex (Liao and Yen, 2008), suggesting a long-lasting abnormality in vascular reactivity in the thalamo-cortical-thalamic circuitry. Similarly, BBB leakage was most evident shortly after TBI in the human brain, but could also be detected months-years after TBI.

Hippocampal BBB damage occurring within minutes to hours after FPI has been described using histochemical and immunohistochemical techniques (Fukuda et al., 1995; Hicks et al., 1997; Schmidt and Grady, 1993). We analyzed Gd-leakage in the hippocampus both in its septal and temporal (data not shown) ends, but found no increased leakage at any time point. We assume this due to a lower sensitivity of the in vivo Gd-MRI technique as compared to histological HRP, IgG, or albumin stainings followed by microscopic analysis.

Taken together, lateral FPI induced a chronic multifocal BBB impairment, which showed a region-specific evolution particularly in the perilesional cortex and ipsilateral thalamus. These data suggest a long-lasting therapeutic window for compounds aimed to mitigate BBB repair and consequent functional impairments.

4.2. BBB dysfunction in relation to brain inflammation

Previous studies have demonstrated chronic neuroinflammation after experimental and human TBI (Webster et al., 2017). Here, we show correlation between the Gd-leakage and CD68 expression in macrophages/monocytes/microglia within the perilesional cortex even at 11 months post-injury. We also found a close proximity between focal thalamic BBB impairment, RECA-1 immunoreactivity and CD68-positive cells, suggesting that continuing BBB leakage is a factor contributing to focal neuroinflammation. Furthermore, neuroinflammation can, in turn, contribute to further BBB damage creating a vicious cycle. In this respect, it is also interesting to investigate other neuropathological alterations, including amyloid plaques and tangles (consisting of hyperphosphorylated tau) which have also shown to be present in this TBI model (Hoshino et al., 1998).

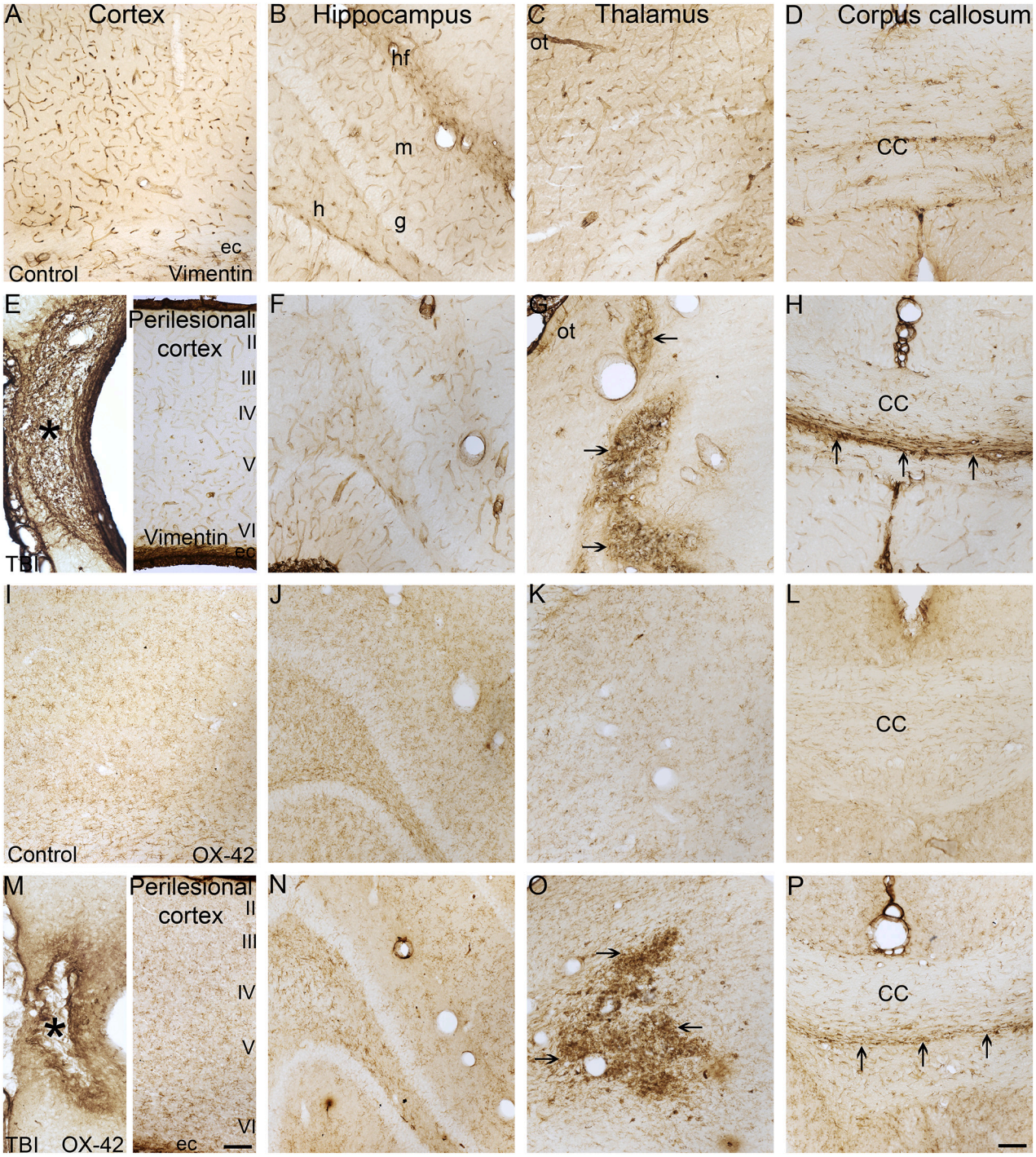

Fig. 9. Vimentin-positive vascular staining and OX-42-positive microglial staining at 11 months after traumatic brain injury (TBI). (A–D) Brightfield photomicrographs of coronal sections demonstrating the distribution of *vimentin immunoreactivity* in the ipsilateral cortex, hippocampus, thalamus, and corpus callosum in a sham-operated control rat. Vimentin labeling was present in blood vessels in all areas. (*E*-H) Vimentin immunoreactivity in a TBI animal. Strong labeling was observed in and around the lesion core (asterisk in E). In the perilesional cortex (E) and hippocampus (F), vimentin immunoreactivity was typically present in blood vessels. In the thalamus (G), there was strong vimentin immunoreactivity in regions presenting calcifications (arrows). Strong vimentin immunoreactivity was also observed in the mid-portion of the corpus callosum (arrows in H). (I–L) OX-42 positive microglia in a sham-operated control rat. OX-42 immuno-positive cells were observed in all the areas. (M-P) *OX-42 immunoreactivity* in a TBI animal. Strong OX-42 immunoreactivity was present in and around the lesion core (asterisk in E). The distribution of OX-42 immunoreactive cells in the perilesional cortex (right panel in M) and the hippocampus (N) was comparable to that in sham-operated controls. (O) In the thalamus, there was strong OX-42 reactivity within the region containing calcifications (arrows). (P) In the corpus callosum, strong OX-42 reactivity was observed in the mid-portion aspect (arrows). Abbreviations: cc, corpus callosum; g, granule cell layer; h, hilus; m, molecular layer; ot, optic tract; hf, hippocampal fissure. Scale bar equals 100 μm (all panels).

In the human brain, chronic neuroinflammation was also evident after TBI in areas with BBB leakage. Therefore, it seems that these neuropathological mechanisms translate well between human and rat after severe TBI. This is also important for future studies, since it has been pointed out that pathological and pathophysiological characteristics relate to particular TBI phenotypes and their appropriateness for

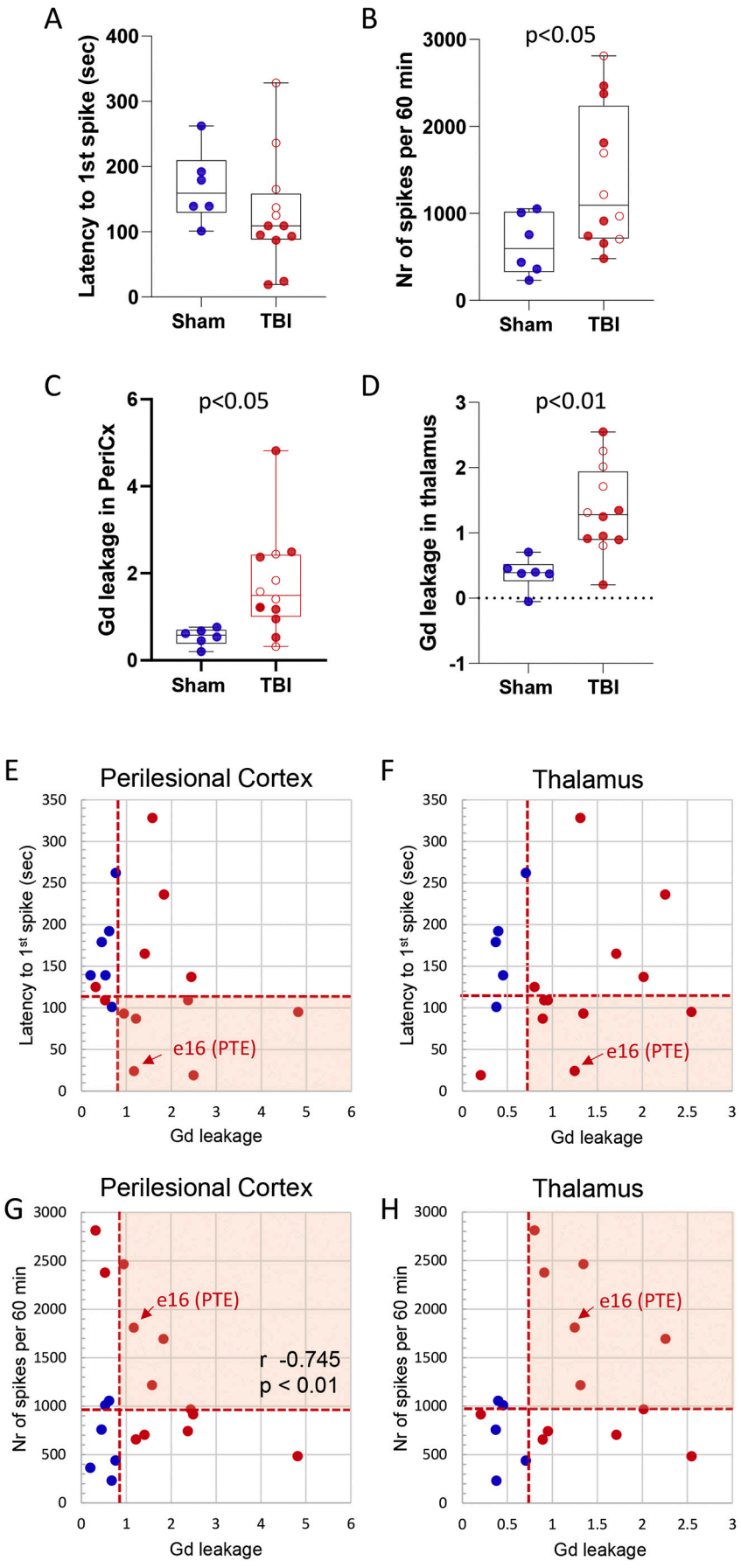

Fig. 10. Chronic gadobutrol (Gd) leakage and seizure susceptibility. Gd-enhanced MRI was performed at 10 months and the PTZ-seizure susceptibility test at 11 months post-TBI. Box plots showing that (A) the latency to the first PTZ-injection -induced spike did not differ between the sham-operated and TBI rats. However, there was a large variability within the TBI group. Consequently, TBI rats with a latency to the first spike at least 1 SD shorter than the mean latency in controls (that is < 113 s) were considered epileptogenic with increased seizure susceptibility (E, filled red circles) and those with ≥113 s non-epileptogenic (Non-E, unfilled red circles) (Nissinen et al., 2017). (B) Number of spikes during the 60 min after PTZ-injection was higher in the TBI group than sham-operated animals. However, there were no difference between the E and Non-E groups. Gd-leakage remained increased even at 10 months post-TBI both in the (C) in the dorsal perilesional cortex (PeriCx, $p < 0.05$) and (D) lateral aspect of the ipsilateral thalamus ($p < 0.01$) as compared to that in the sham-operated control group (blue dots). However, there was no difference between the E and Non-E TBI groups. Scatterplots show the lack of correlation between the increased seizure susceptibility (latency to the first spike in PTZ test, y-axis) and Gd-leakage (x-axis) (E) in the dorsal perilesional cortex (r 0.004, $p > 0.05$) and (F) lateral aspect of the ipsilateral thalamus (r 0.466, $p > 0.05$). Also, there were no correlation between the total number of spikes and Gd-leakage in the (G) perilesional cortex or (H) lateral aspect of the ipsilateral thalamus. Shaded area indicates the increased seizure susceptibility in the PTZ test and increased Gd-leakage in MRI. (For interpretation of the references to colour in this figure legend, the reader is referred to the web version of this article.)

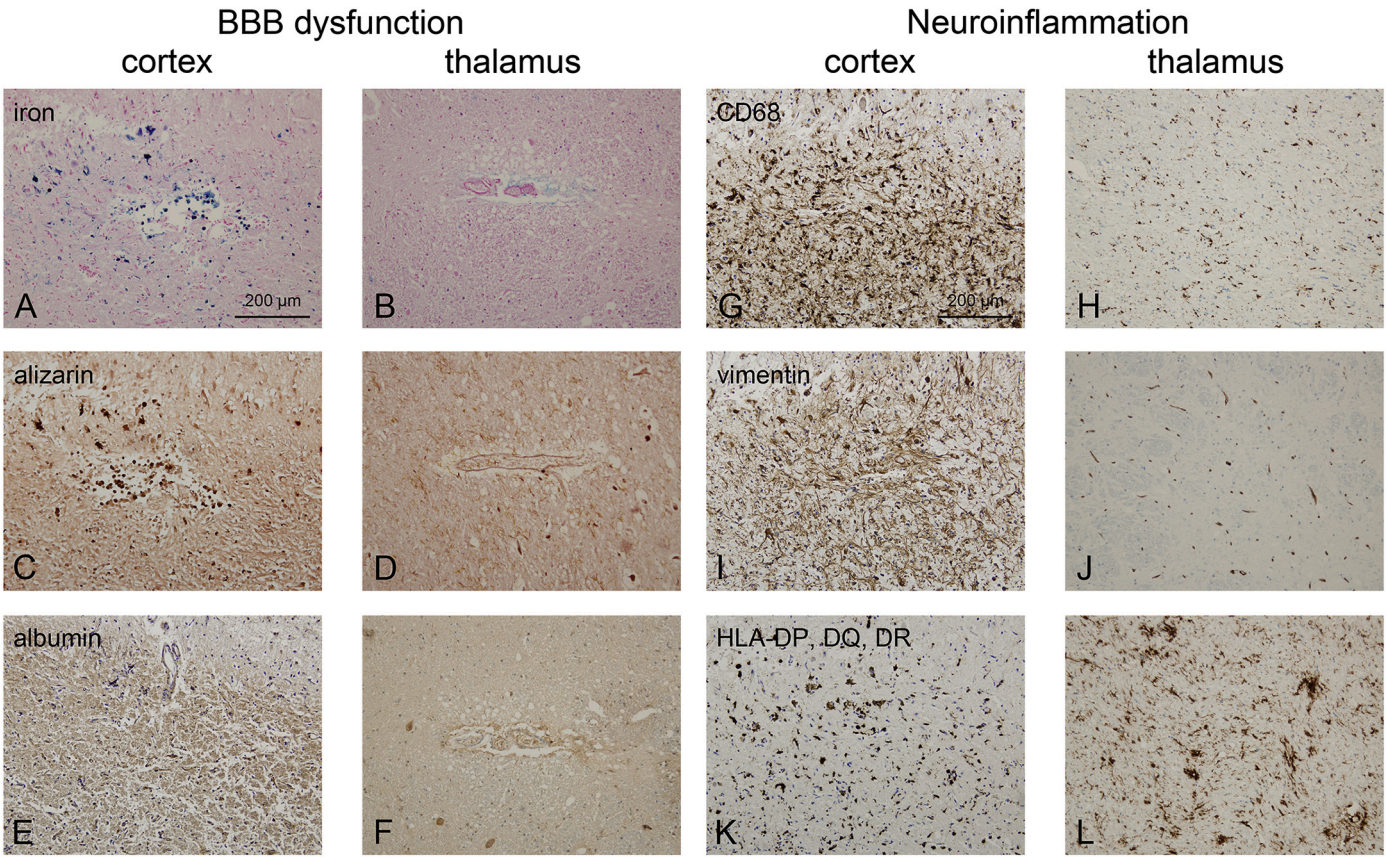

Fig. 11. BBB dysfunction and inflammation in human brain after TBI. The presence of iron (blue) in the (A) cortex and (B) thalamus, calcifications (dark brown) in the (C) cortex and (D) thalamus, and albumin (brown) in the (E) cortex and (F) thalamus in a patient that died 6 months after TBI indicates presence of chronic BBB dysfunction. Furthermore, neuroinflammation was evident in these brain regions as demonstrated by an increase in (G-H) CD68 (activated macrophages/monocytes/microglia), (I-J) vimentin (activated astrocytes), and (K-L) HLA-DP, DQ,DR (activated microglia) immunoreactivity. (For interpretation of the references to colour in this figure legend, the reader is referred to the web version of this article.)

drug testing (Hall, 2016).

In correlation with our previous study at 6 months post-TBI (Lehto et al., 2012), we found calcifications in the thalamus which were surrounded by tortuous RECA-1 positive blood vessels, accumulation of neuroinflammatory markers and Gd-leakage. These data show that calcifications are long-lasting, and imaging could pinpoint the regions of BBB-leakage and chronic neuroinflammation. We also found calcifications in humans with TBI. However, in humans the calcifications were detected in the cerebral cortex, whereas in the rat model the calcifications are almost exclusively described in the thalamus, so far (Lehto et al., 2012; Osteen et al., 2001; Schweser et al., 2019).

4.3. BBB dysfunction and inflammation in relation to seizure susceptibility

Previous studies have elegantly demonstrated that focal BBB-leakage -related albumin entry into the perivascular space can induce astrocytic transforming growth factor beta (TGFβ) signaling, leading to compromised inhibitory neurotransmission (Kim et al., 2017). Frey et al. (2014) showed that the greater the BBB leakage during the first post-injury week, the higher the kainate-induced hyperexcitability at 3 months after lateral FPI in rats. Studies in humans with TBI demonstrated that the area of BBB Gd-leakage rather than the area of TBI lesion was linked to presence of PTE (Tomkins et al., 2011, 2008). Finally, losartan, an anti-hypertensive drug blocking TGFβ signaling was reported to mitigate SE-induced epileptogenesis in rats (Bar-Klein et al., 2014). In the present study, 56% of the TBI rats showed increased seizure susceptibility in the PTZ-test. However, we were not able to demonstrate any association between increased cortical, thalamic or hippocampal Gd-leakage and seizure susceptibility or occurrence/severity PTE as only 1 of the 12 TBI rats had epilepsy. Also, seizure susceptibility was not associated with the severity of neuroinflammation, another factor linked to epileptogenesis (Vezzani et al., 2002).

The present findings oppose the previous finding in several models of SE-induced epileptogenesis and human epilepsy, which have suggested association between the severity of epilepsy and BBB permeability (van Vliet et al., 2014a). We expected to find spontaneous unprovoked seizures (Kharatishvili et al., 2006). However, only 1 of the 12 rats video-EEG-monitored for 3 weeks on the 11th month post-TBI was epileptic, making it impossible to assess the link between the BBB permeability and incidence of epilepsy. Moreover, as we and others have shown, seizure frequency in epilepsy after lateral FPI is low as compared to that in SE-induced epileptogenesis, being 3 seizures in 3 weeks in the present study (Kharatishvili et al., 2006; Nissinen et al., 2017; Shultz et al., 2013). The reasons for this are unknown, but could be due to the fact that rats typically show behavioral features of a non-convulsive SE after lateral TBI (Andrade et al., 2019) rather than a convulsive SE that is observed in most post-SE models. Whether that is less damaging to the brain, and consequently leads to a lower percentage of epilepsy cases as suggested by Young and Claassen (2010), remains to be studied. The low number of animals with spontaneous recurrent seizures in the present study may also be due to repeated anesthesia with isoflurane, which has shown to be antiepileptogenic (Bar-Klein et al., 2016). However, 56% of the TBI rats showed increased seizure susceptibility in the PTZ-test, which can be used to discriminate between epileptogenic and non-epileptogenic rats. This suggests that part of the animals could have developed epilepsy later in life and that the EEG follow-up may be too short. Thus, unless robust BBB leakage had induced a substantially more severe epilepsy in TBI animals, it had

been difficult to demonstrate association between BBB leakage and epilepsy severity. Interestingly, all rats had chronic BBB leakage, while the majority did not have epilepsy.

We studied only male rats, to exclude effects of hormonal variations on BBB leakage, neuroinflammation and epileptogenesis after TBI. However, it is also important to study this in female rats, which will be done in future studies.

Behavioral consequences of TBI are also important. This has been studied extensively in previous studies and our primary focus was the neuropathological outcome (BBB leakage and neuroinflammation) and the correlation with epilepsy. Since we did not find a correlation between these factors, we decided not to perform further behavioral experiments.

As has been shown in our previous studies, as well as by many others (for review see van Vliet et al., 2015), seizures may contribute to BBB damage. Therefore, we have chosen to perform continuous (24/7) video-EEG recordings for 2 weeks before PTZ injections were given. We have previously shown that the BBB leakage can be detected until 1 h after a seizure has occurred (Van Vliet et al., 2007). However, there was only 1 rat that had spontaneous seizures with a low frequency in the present study. Therefore, we do not expect that this has a huge impact. This is confirmed by our results, since this rat had less BBB leakage as compared to rats without seizures (see Fig. 6H and I).

Taken together, our data does not support the idea that chronic BBB-leakage and concomitant focal neuroinflammation are associated with increased incidence or severity of PTE.

5. Conclusion

Our data show chronic BBB dysfunction and neuroinflammation in rat and human perilesional cortex and thalamus after TBI. We were not able to demonstrate an association between BBB impairment and seizure susceptibility or epilepsy in this (relatively small) cohort of animals. However, our data suggest that for treatments aimed to mitigate BBB damage and its secondary pathologies like chronic neuroinflammation, there is a region-specific, long-lasting therapeutic time window. Since these neuropathological processes are both evident in the human and rat brain after TBI, the rat model seems to be suitable to study the effects of novel therapeutic strategies that may later be translated into the clinic.

Funding

The research leading to these results has received funding from the European Union's Seventh Framework Programme (FP7/2007-2013) under grant agreement n°602102 (EPITARGET; EAvV, EA, JAG, AP), the Medical Research Council of the Academy of Finland (Grants 272249, 273909, and 2285733-9)(AP), the Sigrid Juselius Foundation (AP), the Dutch Epilepsy Foundation, project number 16-05 (EAvV), and COST Action BM1001 “Brain Extracellular Matrix in Health and Disease” (ECMnet; EAvV, JAG, EA, AP). .

Acknowledgements

We thank Jarmo Hartikainen and Merja Lukkari for their excellent technical assistance.

Appendix A. Supplementary data

Supplementary data to this article can be found online at https://doi.org/10.1016/j.nbd.2020.105080.

References

Anderson, C.V., Wood, D.-M.G., Bigler, E.D., Blatter, D.D., 1996. Lesion volume, injury severity, and thalamic integrity following head injury. J. Neurotrauma 13, 59–65. https://doi.org/10.1089/neu.1996.13.59.

Andrade, P., Paananen, T., Ciszek, R., Lapinlampi, N., Pitkänen, A., 2018. Algorithm for automatic detection of spontaneous seizures in rats with post-traumatic epilepsy. J. Neurosci. Methods 307. https://doi.org/10.1016/j.jneumeth.2018.06.015.

Andrade, P., Banuelos-Cabrera, I., Lapinlampi, N., Paananen, T., Ciszek, R., Ndode-Ekane, X.E., Pitkänen, A., 2019. Acute non-convulsive status epilepticus after experimental traumatic brain injury in rats. J. Neurotrauma 36, 1890–1907. https://doi.org/10.1089/neu.2018.6107.

Annegers, J.F., Hauser, W.A., Coan, S.P., Rocca, W.A., 1998. A population-based study of seizures after traumatic brain injuries. N. Engl. J. Med. 338, 20–24. https://doi.org/10.1056/NEJM199801013380104.

Bar-Klein, G., Cacheaux, L.P., Kamintsky, L., Prager, O., Weissberg, I., Schoknecht, K., Cheng, P., Kim, S.Y., Wood, L., Heinemann, U., Kaufer, D., Friedman, A., 2014. Losartan prevents acquired epilepsy via TGF-β signaling suppression. Ann. Neurol. 75, 864–875. https://doi.org/10.1002/ana.24147.

Bar-Klein, G., Klee, R., Brandt, C., Bankstahl, M., Bascuñana, P., Töllner, K., Dalipaj, H., Bankstahl, J.P., Friedman, A., Löscher, W., Friedman, A., 2016. Isoflurane prevents acquired epilepsy in rat models of temporal lobe epilepsy. Ann. Neurol. 80, 896–908. https://doi.org/10.1002/ana.24804.

Bar-Klein, G., Lublinsky, S., Kamintsky, L., Noyman, I., Veksler, R., Dalipaj, H., Senatorov, V.V., Swissa, E., Rosenbach, D., Elazary, N., Milikovsky, D.Z., Milk, N., Kassirer, M., Rosman, Y., Serlin, Y., Eisenkraft, A., Chassidim, Y., Parmet, Y., Kaufer, D., Friedman, A., 2017. Imaging blood-brain barrier dysfunction as a biomarker for epileptogenesis. Brain 140, 1692–1705. https://doi.org/10.1093/brain/awx073.

Frey, L., Lepkin, A., Schickedanz, A., Huber, K., Brown, M.S., Serkova, N., 2014. ADC mapping and T1-weighted signal changes on post-injury MRI predict seizure susceptibility after experimental traumatic brain injury. Neurol. Res. 36, 26–37. https://doi.org/10.1179/1743132813Y.0000000269.

Fukuda, K., Tanno, H., Okimura, Y., Nakamura, M., Yamaura, A., 1995. The blood–brain barrier disruption to circulating proteins in the early period after fluid percussion brain injury in rats. J. Neurotrauma 12, 315–324. https://doi.org/10.1089/neu.1995.12.315.

Hall, E.D., 2016. Translational principles of neuroprotective and neurorestorative therapy testing in animal models of traumatic brain injury. In: Laskowitz, D.G.G. (Ed.), Translational Research in Traumatic Brain Injury. CRC Press/Taylor and Francis Group, Boca Raton, pp. 239–262.

Hicks, R.R., Baldwin, S.A., Scheff, S.W., 1997. Serum extravasation and cytoskeletal alterations following traumatic brain injury in rats. Mol. Chem. Neuropathol. 32, 1–16. https://doi.org/10.1007/BF02815164.

Hoshino, S., Tamaoka, A., Takahashi, M., Kobayashi, S., Furukawa, T., Oaki, Y., Mori, O., Matsuno, S., Shoji, S., Inomata, M., Teramoto, A., 1998. Emergence of immunoreactivities for phosphorylated tau and amyloid-β protein in chronic stage of fluid percussion injury in rat brain. Neuroreport 9, 1879–1883. https://doi.org/10.1097/00001756-199806010-00039.

Immonen, R.J., Kharatishvili, I., Gröhn, H., Pitkänen, A., Gröhn, O.H.J., 2009. Quantitative MRI predicts long-term structural and functional outcome after experimental traumatic brain injury. Neuroimage 45. https://doi.org/10.1016/j.neuroimage.2008.11.022.

Ivens, S., Kaufer, D., Flores, L.P., Bechmann, I., Zumsteg, D., Tomkins, O., Seiffert, E., Heinemann, U., Friedman, A., 2007. TGF- receptor-mediated albumin uptake into astrocytes is involved in neocortical epileptogenesis. Brain 130, 535–547. https://doi.org/10.1093/brain/awl317.

Kadam, S.D., D'Ambrosio, R., Duveau, V., Roucard, C., Garcia-Cairasco, N., Ikeda, A., de Curtis, M., Galanopoulou, A.S., Kelly, K.M., 2017. Methodological standards and interpretation of video-electroencephalography in adult control rodents. A TASK1-WG1 report of the AES/ILAE Translational Task Force of the ILAE. Epilepsia 58, 10–27. https://doi.org/10.1111/epi.13903.

Kharatishvili, I., Nissinen, J.P., McIntosh, T.K., Pitkänen, A., 2006. A model of post-traumatic epilepsy induced by lateral fluid-percussion brain injury in rats. Neuroscience 140, 685–697. https://doi.org/10.1016/j.neuroscience.2006.03.012.

Kharatishvili, I., Immonen, R., Gröhn, O., Pitkänen, A., 2007. Quantitative diffusion MRI of hippocampus as a surrogate marker for post-traumatic epileptogenesis. Brain 130. https://doi.org/10.1093/brain/awm268.

Kim, H., Yu, T., Cam-Etoz, B., van Groen, T., Hubbard, W.J., Chaudry, I.H., 2017. Treatment of traumatic brain injury with 17α-ethinylestradiol-3-sulfate in a rat model. J. Neurosurg. 127, 23–31. https://doi.org/10.3171/2016.7.JNS161263.

Kim, S., Mortera, M., Hu, X., Krishnan, S., Hoffecker, L., Herrold, A., Terhorst, L., King, L., Machtinger, J., Zumsteg, J.M., Negm, A., Heyn, P., 2019. Overview of pharmacological interventions after traumatic brain injuries: impact on selected outcomes. Brain Inj. 33, 442–455. https://doi.org/10.1080/02699052.2019.1565896.

Lehto, L.J., Sierra, A., Corum, C.A., Zhang, J., Idiyatullin, D., Pitkänen, A., Garwood, M., Gröhn, O., 2012. Detection of calcifications in vivo and ex vivo after brain injury in rat using SWIFT. Neuroimage 61, 761–772. https://doi.org/10.1016/j.neuroimage.2012.03.002.

Lewis, D.A., Campbell, M.J., Morrison, J.H., 1986. An immunohistochemical characterization of somatostatin-28 and somatostatin-281-12 in monkey prefrontal cortex. J. Comp. Neurol. 248, 1–18. https://doi.org/10.1002/cne.902480102.

Liao, C.-C., Yen, C.-T., 2008. Functional connectivity of the secondary somatosensory cortex of the rat. Anat. Rec. Adv. Integr. Anat. Evol. Biol. 291, 960–973. https://doi.org/10.1002/ar.20696.

Lin, Y., Pan, Y., Wang, M., Huang, X., Yin, Y., Wang, Y., Jia, F., Xiong, W., Zhang, N., Jiang, J.Y., 2012. Bloodbrain barrier permeability is positively correlated with cerebral microvascular perfusion in the early fluid percussion-injured brain of the rat. Lab. Investig. 92, 1623–1634. https://doi.org/10.1038/labinvest.2012.118.

Marklund, N., Hillered, L., 2011. Animal modelling of traumatic brain injury in preclinical drug development: where do we go from here? Br. J. Pharmacol. 164,

1207–1229. https://doi.org/10.1111/j.1476-5381.2010.01163.x.
McIntosh, T.K., Vink, R., Noble, L., Yamakami, I., Fernyak, S., Soares, H., Faden, A.L., 1989. Traumatic brain injury in the rat: characterization of a lateral fluid-percussion model. Neuroscience 28, 233–244. https://doi.org/10.1016/0306-4522(89)90247-9.
Menon, D.K., Schwab, K., Wright, D.W., Maas, A.I., Demographics and Clinical Assessment Working Group of the International and Interagency Initiative toward Common Data Elements for Research on Traumatic Brain Injury and Psychological Health, 2010. Position statement: definition of traumatic brain injury. Arch. Phys. Med. Rehabil. 91, 1637–1640. https://doi.org/10.1016/j.apmr.2010.05.017.
Michalak, Z., Lebrun, A., Di Miceli, M., Rousset, M.-C., Crespel, A., Coubes, P., Henshall, D.C., Lerner-Natoli, M., Rigau, V., 2012. IgG leakage may contribute to neuronal dysfunction in drug-refractory epilepsies with blood-brain barrier disruption. J. Neuropathol. Exp. Neurol. 71, 826–838. https://doi.org/10.1097/NEN.0b013e31826809a6.
Nissinen, J., Andrade, P., Natunen, T., Hiltunen, M., Malm, T., Kanninen, K., Soares, J.I., Shatillo, O., Sallinen, J., Ndode-Ekane, X.E., Pitkänen, A., 2017. Disease-modifying effect of atipamezole in a model of post-traumatic epilepsy. Epilepsy Res. 136, 18–34. https://doi.org/10.1016/j.eplepsyres.2017.07.005.
Obermeier, B., Verma, A., Ransohoff, R.M., 2016. The Blood–Brain Barrier. pp. 39–59. https://doi.org/10.1016/B978-0-444-63432-0.00003-7.
Osteen, C.L., Moore, A.H., Prins, M.L., Hovda, D.A., 2001. Age-dependency of 45 calcium accumulation following lateral fluid percussion: acute and delayed patterns. J. Neurotrauma 18, 141–162. https://doi.org/10.1089/08977150150502587.
Paxinos, G., Watson, C., 2007. The Rat Brain in Stereotaxic Coordinates, 6th ed. Academic Press.
Perry, D.C., Sturm, V.E., Peterson, M.J., Pieper, C.F., Bullock, T., Boeve, B.F., Miller, B.L., Kevin, M., Berger, M.S., Kramer, J.H., Kathleen, A., 2017. and psychiatric disease: a meta-analysis. 124, 511–526. https://doi.org/10.3171/2015.2.JNS14503. Traumatic.
Pitkänen, A., McIntosh, T.K., 2006. Animal models of post-traumatic epilepsy. J. Neurotrauma 23, 241–261. https://doi.org/10.1089/neu.2006.23.241.
Racine, R.J., 1972. Modification of seizure activity by electrical stimulation: II. Motor seizure. Electroencephalogr. Clin. Neurophysiol. 32, 281–294. https://doi.org/10.1016/0013-4694(72)90177-0.
Ramlackhansingh, A.F., Brooks, D.J., Greenwood, R.J., Bose, S.K., Turkheimer, F.E., Kinnunen, K.M., Gentleman, S., Heckemann, R.A., Gunanayagam, K., Gelosa, G., Sharp, D.J., 2011. Inflammation after trauma: microglial activation and traumatic brain injury. Ann. Neurol. 70, 374–383. https://doi.org/10.1002/ana.22455.
Rodgers, K.M., Dudek, F.E., Barth, D.S., 2015. Progressive, seizure-like, spike-wave discharges are common in both injured and uninjured Sprague-Dawley rats: implications for the fluid percussion injury model of post-traumatic epilepsy. J. Neurosci. 35, 9194–9204. https://doi.org/10.1523/JNEUROSCI.0919-15.2015.
Salehi, A., Zhang, J.H., Obenaus, A., 2017. Response of the cerebral vasculature following traumatic brain injury. J. Cereb. Blood Flow Metab. 37, 2320–2339. https://doi.org/10.1177/0271678X17701460.
Sandsmark, D.K., Bashir, A., Wellington, C.L., Diaz-Arrastia, R., 2019. Cerebral microvascular injury: a potentially treatable endophenotype of traumatic brain injury-induced neurodegeneration. Neuron 103, 367–379. https://doi.org/10.1016/j.neuron.2019.06.002.
Schmidt, R.H., Grady, M.S., 1993. Regional patterns of blood–brain barrier breakdown following central and lateral fluid percussion injury in rodents. J. Neurotrauma 10, 415–430. https://doi.org/10.1089/neu.1993.10.415.
Schneider, G., Fries, P., Wagner-Jochem, D., Thome, D., Laurer, H., Kramann, B., Mautes, A., Hagen, T., 2002. Pathophysiological changes after traumatic brain injury: comparison of two experimental animal models by means of MRI. Magma Magn. Reson. Mater. Phys. Biol. Med. 14, 233–241. https://doi.org/10.1007/BF02668217.
Schweser, F., Kyyriäinen, J., Preda, M., Pitkänen, A., Toffolo, K., Poulsen, A., Donahue, K., Levy, B., Poulsen, D., 2019. Visualization of thalamic calcium influx with quantitative susceptibility mapping as a potential imaging biomarker for repeated mild traumatic brain injury. Neuroimage 200, 250–258. https://doi.org/10.1016/j.neuroimage.2019.06.024.
Shlosberg, D., Benifla, M., Kaufer, D., Friedman, A., 2010. Blood-brain barrier breakdown as a therapeutic target in traumatic brain injury. Nat. Rev. Neurol. 6, 393–403. https://doi.org/10.1038/nrneurol.2010.74.
Shultz, S.R., Cardamone, L., Liu, Y.R., Hogan, R.E., Maccotta, L., Wright, D.K., Zheng, P., Koe, A., Gregoire, M.-C., Williams, J.P., Hicks, R.J., Jones, N.C., Myers, D.E., O'Brien, T.J., Bouilleret, V., 2013. Can structural or functional changes following traumatic brain injury in the rat predict epileptic outcome? Epilepsia 54, 1240–1250. https://doi.org/10.1111/epi.12223.
Smith, D.H., Chen, X.H., Pierce, J.E., Wolf, J.A., Trojanowski, J.Q., Graham, D.I., McIntosh, T.K., 1997. Progressive atrophy and neuron death for one year following brain trauma in the rat. J. Neurotrauma 14, 715–727. https://doi.org/10.1089/neu.1997.14.715.
Taylor, J.A., Rodgers, K.M., Bercum, F.M., Booth, C.J., Dudek, F.E., Barth, D.S., 2017. Voluntary control of epileptiform spike–wave discharges in awake rats. J. Neurosci. 37, 5861–5869. https://doi.org/10.1523/JNEUROSCI.3235-16.2017.
Taylor, J.A., Reuter, J.D., Kubiak, R.A., Mufford, T.T., Booth, C.J., Dudek, F.E., Barth, D.S., 2019. Spontaneous recurrent absence seizure-like events in wild-caught rats. J. Neurosci. 39, 4829–4841. https://doi.org/10.1523/JNEUROSCI.1167-18.2019.
Thal, S.C., Neuhaus, W., 2014. The blood-brain barrier as a target in traumatic brain injury treatment. Arch. Med. Res. 45, 698–710. https://doi.org/10.1016/j.arcmed.2014.11.006.
Tomkins, O., Shelef, I., Kaizerman, I., Eliushin, A., Afawi, Z., Misk, A., Gidon, M., Cohen, A., Zumsteg, D., Friedman, A., 2008. Blood-brain barrier disruption in post-traumatic epilepsy. J. Neurol. Neurosurg. Psychiatry 79, 774–777. https://doi.org/10.1136/jnnp.2007.126425.
Tomkins, O., Feintuch, A., Benifla, M., Cohen, A., Friedman, A., Shelef, I., 2011. Blood-brain barrier breakdown following traumatic brain injury: a possible role in post-traumatic epilepsy. Cardiovasc. Psychiatry Neurol. 2011, 765923. https://doi.org/10.1155/2011/765923.
Van Vliet, E.A., Araújo, S.D.C., Redeker, S., Van Schaik, R., Aronica, E., Gorter, J.A., 2007. Blood-brain barrier leakage may lead to progression of temporal lobe epilepsy. Brain 130, 521–534. https://doi.org/10.1093/brain/awl318.
van Vliet, E.A., Aronica, E., Gorter, J.A., 2014a. Role of blood-brain barrier in temporal lobe epilepsy and pharmacoresistance. Neuroscience 277, 455–473. https://doi.org/10.1016/j.neuroscience.2014.07.030.
van Vliet, E.A., Otte, W.M., Gorter, J.A., Dijkhuizen, R.M., Wadman, W.J., 2014b. Longitudinal assessment of blood–brain barrier leakage during epileptogenesis in rats. A quantitative MRI study. Neurobiol. Dis. 63, 74–84. https://doi.org/10.1016/j.nbd.2013.11.019.
van Vliet, E.A., Aronica, E., Gorter, J.A., 2015. Blood-brain barrier dysfunction, seizures and epilepsy. Semin. Cell Dev. Biol. 38, 26–34. https://doi.org/10.1016/j.semcdb.2014.10.003.
Vezzani, A., Moneta, D., Richichi, C., Aliprandi, M., Burrows, S.J., Ravizza, T., Perego, C., De Simoni, M.G., 2002. Functional role of inflammatory cytokines and antiinflammatory molecules in seizures and epileptogenesis. Epilepsia 43, 30–35. https://doi.org/10.1046/j.1528-1157.43.s.5.14.x.
Webster, K.M., Sun, M., Crack, P., O'Brien, T.J., Shultz, S.R., Semple, B.D., 2017. Inflammation in epileptogenesis after traumatic brain injury. J. Neuroinflammation 14, 10. https://doi.org/10.1186/s12974-016-0786-1.
Xiong, Y., Mahmood, A., Chopp, M., 2013. Animal models of traumatic brain injury. Nat. Rev. Neurosci. 14, 128–142. https://doi.org/10.1038/nrn3407.
Yasmin, A., Pitkänen, A., Jokivarsi, K., Poutiainen, P., Gröhn, O., Immonen, R., 2019. MRS reveals chronic inflammation in T2w MRI-negative perilesional cortex – a 6-months multimodal imaging follow-up study. Front. Neurosci. 13. https://doi.org/10.3389/fnins.2019.00863.
Young, G.B., Claassen, J., 2010. Nonconvulsive status epilepticus and brain damage: further evidence, more questions. Neurology 75, 760–761. https://doi.org/10.1212/WNL.0b013e3181f32141.